Role of *cct3* in Schwann cells survival, neuromuscular junction formation as well as axonal microtubule biology and axonal transport

Von der Medizinischen Fakultät
der Rheinisch-Westfälischen Technischen Hochschule Aachen
zur Erlangung des akademischen Grades einer Doktorin der Medizin genehmigte Dissertation

vorgelegt von

Master of Neurology

Xiaomeng Zhang

aus Weifang (China)

Berichter: Jun.-Prof. Dr. med. Dr. sc. nat. Juliane Bremer
Univ.-Prof. Dr. med. Ingo Kurth

Tag der mündlichen Prüfung: 17.03.2026

Diese Dissertation ist auf den Internetseiten der Universitätsbibliothek online verfügbar.

Parts of this dissertation have been provisionally accepted for publication as the following manuscript in a peer-reviewed journal:

X. Zhang*, K. K. Zajt*, T. Palaz, L. Wang, M. Groß, F. Kraft, J. Weis, J. Bremer.: The chaperonin TRiC component Cct3 is required for axonal transport, myelination and neuromuscular junction refinement.
Provisionally accepted in January 2026 at the Journal “Cell Death and Disease”
(* these authors contributed equally to this work)

Table of Content

Table of Content II
List of Figures VIII
List of Tables..... X
List of Abbreviations..... XI
1 Introduction 1
1.1 Chaperonin tailless complex polypeptide 1 ring complex (TRiC)..... 1
1.1.1 The structure and function of TRiC/CCT 2
1.1.2 TRiC/CCT and neurodegenerative diseases..... 4
1.2 Myelin sheath..... 8
1.2.1 The function of myelin sheath 8
1.2.2 Development of myelin in the peripheral nervous system..... 15
1.2.3 Development of myelin in the central nervous system..... 17
1.3 Microtubules – a main component of the cytoskeleton..... 21
1.3.1 The structure of microtubules 21
1.3.2 The function of microtubules..... 23
1.3.3 Microtubule dynamics 27

1.3.4 Microtubule-binding proteins (MTBPs)..... 30
1.3.4.1 Microtubule-associated proteins (MAPs) 31
1.3.4.2 Plus-end tracking proteins (+TIPs)..... 33
1.3.4.3 Motor proteins..... 35
1.4 Axonal transport..... 37
1.4.1 Anterograde transport..... 38
1.4.2 Retrograde transport..... 38
2 Research Objective..... 39
3 Materials and Methods..... 42
3.1 Materials 42
3.1.1 Zebrafish lines 42
3.1.1.1 Wildtype fishline..... 43
3.1.1.2 Mutants fishlines..... 43
3.1.1.3 Transgenic fishlines..... 44
3.1.2 Oligonucleotides (Primers)..... 45
3.1.3 Buffers and solutions 46
3.1.4 Media..... 48
3.1.5 Kits..... 50
3.1.6 Enzymes..... 51
3.1.7 Antibodies..... 51

3.1.8 Bacteria 53
3.1.9 General Reagents 53
3.1.10 Consumables 55
3.1.11 Software and Devices 56
3.1.12 Artificial Intelligence/ChatGPT ... 57
3.2 Methods 57
3.2.1 Zebrafish related methods 57
3.2.1.1 Zebrafish Housing and Husbandry 58
3.2.1.2 Mating procedure 61
3.2.1.3 Fin biopsies 61
3.2.1.4 Live imaging and time-lapse microscopy 62
3.2.1.5 Immunostaining 64
3.2.1.5.1 BTX Staining 64
3.2.1.5.2 Acetylated/ glutamylated tubulin staining 65
3.2.1.5.3 Activated Casp3 Immunolabeling 66
3.2.1.6 Western Blot 67
3.2.1.7 Cct3 mRNA injection 69
3.2.2 Molecular methods 70

3.2.2.1 DNA Extraction from caudal fin 70
3.2.2.2 PCR with GoTaq® DNA Polymerase 70
3.2.2.3 Pfu-PCR with PfuTurbo DNA Polymerase 71
3.2.2.4 Restriction Enzyme Disgestion 72
3.2.2.5 Gel electrophoresis..... 73
3.2.2.6 Plasmid-related methods..... 73
3.2.2.6.1 TOPO TA Cloning 73
3.2.2.6.2 Chemical Transformation . 74
3.2.2.6.3 Mini preparation..... 74
3.2.2.6.4 Midi Preparation 76
3.2.2.7 *In vitro* RNA synthesis 78
3.2.2.7.1 DNA extraction from agarose gels and purification of DNA 78
3.2.2.7.2 *In vitro* RNA synthesis and purification..... 80
3.2.2.7.3 Agarose RNA gel electrophoresis..... 81
3.2.2.7.4 Sequencing 82

4 Results 83
4.1 Characterization of cct3 loss-of-function allele 83
4.1.1 Compound heterozygous cct3 mutation-induced phenotype..... 83
4.1.2 Cct3 protein was undetectable in *cct3* mutants 85
4.1.3 Cct3-deficient larvae show reduced response to mechanical stimulation..... 86
4.1.4 Wildtype *cct3* mRNA rescues the phenotype of *cct3* mutants..... 87
4.1.5 Apoptotic Schwann cells in *cct3* mutants 89
4.2 *Cct3* mutants influence the function of microtubule 93
4.2.1 Tubulin was undetectable in cct3 mutants 93
4.2.2 Altered posttranslational modifications of tubulin were in *cct3* mutants 94
4.2.3 The distribution of microtubule was disrupted in *cct3* mutants 96

4.3 Developmental refinement of neuromuscular junction and muscle fiber architecture are disturbed in *cct3* mutants 98
4.4 The axonal transport of organelles was disrupted in *cct3* mutants 103
5 Discussion..... 107
6 Summary..... 113
7 References..... 119
List of own publications..... 146
Acknowledgement..... 148
Erklärung zur Datenaufbewahrung 151
Erklärung über den Eigenanteil..... 152
Curriculum Vitae 154

List of Figures

Figure 1. The morphological changes between *cct3* siblings and mutants. 85
Figure 2. Western blot result of cct3 protein. 86
Figure 3. The touch-evoked response reduced in *cct3* mutants. 87
Figure 4. cct3 mRNA rescue the phenotype of *cct3* mutants..... 88
Figure 5. Quantification of the rescue experiment. 89
Figure 6. Live imaging of *Tg(sox10:nlsEOS) tg(Xla.Tubb:DsRed)*. 91
Figure 7. Results of Caspase-3 Assay. 93
Figure 8. Western blot result of actin/tubulin. 94
Figure 9. Results of acetylated/glutamylated tubulin immunostaining. 96
Figure 10. Distribution of F-actin and microtubules..... 98
Figure 11. Results of BTX staining..... 100
Figure 12. Results of phalloidin/vinculin staining. 102
Figure 13. Quantification of BTX staining and phalloidin/vinculin staining. 103

Figure 14. The time lapse images of *Tg(mnx1:Gal4)Tg(UAS:EGFP-Rab7)* at 2, 3, and 4 dpf. 105
Figure 15. The time lapse images of *Tg(mnx1:Gal4) Tg(UAS:mito-mCherry)* 106

List of Tables

Table 1: Wild type (WT) mutant and transgenic zebrafish lines used in this thesis. 42
Table 2: dCAPS oligonucleotides used for genotyping. 45
Table 3: Additional primers 46
Table 4: Buffers and solutions with recipe ... 46
Table 5: Commercial buffers and solutions .. 48
Table 6: Used media with information regarding their composition or manufacturer..... 49
Table7: Commercial kits 50
Table 8: Restriction enzymes..... 51
Table 9: Other enzymes..... 51
Table 10: Antibodies 52
Table 11: General reagents and chemicals . 53
Table 12: Used consumables with information regarding the manufacturer..... 55
Table 13: Used software and devices 56
Table 14: Standard PCR programmes..... 71

List of Abbreviations

+TIPs	Plus-end tracking proteins
AChR	Acetylcholine receptor
AD	Alzheimer's Disease
APP	Amyloid precursor protein
ApiCCT1	the apical domain of CCT1
ALS	Amyotrophic lateral sclerosis
ATAT1	α-tubulin acetyltransferase
ATG8s	Autophagy-related 8 proteins
ATP	Adenosine triphosphate
ATXN3	Ataxin 3
BDNF	Brain-derived neurotrophic factor
BSA	Bovine serum albumin
CaCl2	Calcium chloride
CCPs	Cytosolic carboxy peptidases
CNS	Central nervous system
CPC	Central pair complex
CMS	Congenital Myasthenic Syndromes
CMT	Charcot-Marie-Tooth disease
CNP	Cyclic nucleotide phosphodiesterase

dpf	Days post fertilization
ddH2O	Double distilled water
DMSO	Dimethyl sulfoxide
DMTs	Doublet microtubules
EBs	End-binding proteins
EDTA	Ethylenediaminetetraacetic acid
FTD	Frontotemporal Dementia
GFP	Green fluorescent protein
GDNF	Glial cell line-derived neurotrophic factor
GOIs	Genes-of-interest
GTP	Guanosine triphosphate
HDACs	Histone deacetylases
HRP	Horseradish peroxidase
Hsp	Heatshock protein
Htt	Huntington
IJ	Inner junction
IGF-1	Insulin-like growth factor 1
KCl	Potassium Chloride
KH_2PO_4	Monopotassium phosphate
Lrp4	Low density lipoprotein receptor-related protein 4

M13 fw	M13 forward
M13 rev	M13 reverse
MgCl2	Magnesium chloride
MDa	Mega dalton
MeOH	Methanol
MAPs	Microtubule-associated proteins
MTBPs	Microtubule-binding proteins
MCT1	Monocarboxylate Tansporter 1
MRI	Magnetic resonance imaging
mSOD1	Mouse superoxide dismutase 1
MuSK	Muscle-specific kinase
mHTT	Mutant huntington
MBP	Myelin basic protein
MOG	Myelin oligodendrocyte glycoprotein
MAG	Myelin-associated glycoprotein
Na_2HPO_4	Sodium hydrogen phosphate
NaCl	Sodium chloride
NGF	Nerve growth factor

NSCs	Neural stem cells
Nogo-A	Neurite outgrowth inhibitor-A
NFTs	Neurofibrillary tangles
NGS	Normal goat serum
NMJs	Neuromuscular junctions
N site	Nonexchangeable site
OMGp	Oligodendrocyte myelin glycoprotein
OPCs	Oligodendrocyte precursor cells
OLs	Oligodendrocytes
ON	Overnight
OJ	Outer junction
p53	Tumor protein p53
PFA	Paraformaldehyde
PBS	Phosphate buffered saline
PCR	Polymerase chain reaction
PNS	Peripheral nervous system
PEX7	Peroxisomal biogenesis factor 7
Pfu	Pyrococcus furiosus
PK	Proteinase K

PTMs	Post-translational modifications
PLP	proteolipid protein
PSP	Progressive supranuclear palsy
RE	Restriction enzyme
RFP	Red Fluorescent Protein
RT	Room temperature
SLIs	Schmidt–Lanterman incisures
SCs	Schwann cells
SDS-PAGE	Sodium Dodecyl Sulfate Polyacrylamide Gel Electrophoresis
Sox10	SRY-related hmg-box 10
STAT3	Signal Transducer and Activator of Transcription 3
TBST	Tris-buffered saline with Tween 20
TCP-1	T-complex 1
TRiC/CCT	Chaperonin tailless complex polypeptide 1 ring complex/Chaperonin

	containing tailless complex polypeptide 1
TTLL1	TTL family tubulin polyglutamylase complex subunit L1
VHL	von Hippel-Lindau protein
WB	Western blot
WT	Wild-type
α-BTX	α-bungarotoxin

1 Introduction

1.1 Chaperonin tailless complex polypeptide 1 ring complex (TRiC)

Chaperonin tailless complex polypeptide 1 ring complex (TRiC), also known as Chaperonin containing tailless complex polypeptide 1 (CCT), is a hetero-oligomeric molecular complex and chaperone found in eukaryotic cells (Horovitz et al. 2022; Grantham 2020). Most of cellular functions rely on actions of different proteins. To maintain the protein homeostasis (proteostasis), mammalian cells must ensure that they can effectively fold and assemble different proteins during synthesis. Proteins have very limited stability at physiological temperatures and are constantly at risk of misfolding, and many diseases ranging from cancer to neurodegeneration, are linked to protein misfolding (Gestaut et al. 2022). Therefore, proteostasis is maintained by a variety of factors, including molecular chaperones (Hipp et al. 2014). Chaperones are proteins that assist in the assembly of cellular

macromolecules and help newly synthesized proteins fold into their proper structures. They can utilize the energy derived from ATP hydrolysis to help newly synthesized proteins assume their correct three-dimensional conformations and prevent misfolding (Horovitz et al. 2022; Gestaut et al. 2019). Chaperones have been classified into two groups. Group I is found in prokaryotes (GroEL/GroES), mitochondria (Hsp60/Hsp10), and chloroplasts (Rubisco subunit binding protein). The other is group II, which is found in eukaryotes cytosol (TRiC/CCT) and archaea (thermosome, Mm-cpn) (Horovitz et al. 2022, Gestaut et al. 2019; Jin et al. 2019).

1.1.1 The structure and function of TRiC/CCT

Chaperonin TRiC/CCT (approximately 1 MDa) is composed of eight parallel homologous subunits (CCT1-CCT8, also called CCTα, β, γ, δ, ε, ζ, η, θ) that assemble in a fixed order to form a double-ring structure (Jin et al. 2019).

The two rings stack to create a barrel-shaped chamber, with each ring containing eight different subunits. The CCT1-CCT8 subunits share only 30% sequence similarity but are structurally highly similar, each consisting of three structural domains: an apical domain (A domain) which contains the substrate recognition sites and a loop that forms a lid, an equatorial domain (E domain) which contains the ATP-binding sites and forms the intra- and inter-ring contacts; and an intermediate domain (I domain) which connects the other two domains (Jin et al. 2019; Gestaut et al. 2022).

Coordinated with its ATP-driven conformational cycle, approximately 10% of the proteins in the cell are assisted by the molecular chaperone TRiC, folding within its chamber to achieve their final functional structures, and cytoskeleton proteins such as actin and tubulin are some of its best-known substrates (Jin et al. 2019; Gestaut et al. 2022). What's more, TRiC is also crucial for the folding of many other proteins related to oncogenesis, such as p53, VHL

tumor suppressor, and STAT3, and to the folding of retinal developmental factors, including transducin α and PEX7 (Jin et al. 2019).

1.1.2 TRiC/CCT and neurodegenerative diseases

Since TRiC plays a critical role in the proper folding of numerous proteins involved in oncogenesis and retinal development, impairment of TRiC is closely linked to cancer and neurodegenerative diseases (Jin et al. 2019). Recently, we described a disease spectrum, known as “TRiCopathies”, which is caused by the dysfunction of TRiC and subsequently affects the protein folding in the development of the central nervous system (Kraft et al. 2024). Patients with TRiC impairment often present similar clinical features, including movement disorders, cognitive impairments and disturbances in the peripheral nervous system.

Increasing the expression of CCT8 in somatic tissues has been shown to extend the lifespan of *Caenorhabditis elegans* in a TRiC/CCT-dependent manner (Noormohammadi et al. 2016). Furthermore, ectopic expression of CCT8 improves age-associated decline in proteostasis and corrects proteostatic deficiencies in Huntington's disease worm models (Noormohammadi et al. 2016).

Researchers have revealed that TRiC operates on misfolded proteins though a dual defense mechanism. In the presence of misfolded proteins, TRiC acts as the first line of defense by performing its conventional function to fold these proteins and prevent their aggregation (Ma et al. 2022). When excess misfolded proteins accumulate and form protein aggregates, a portion of CCT2 becomes monomeric and switches its function to the autophagy receptor, serving as a second line of defense to maintain proteostasis (Ma et al. 2022). Specifically, CCT2 functions as an autophagy receptor by binding to ATG8s

through its C-terminal VLIR motif while its apical domain interacts with aggregation-prone proteins to facilitate the autophagic process (Ma et al. 2022). Additionally, CCT2 subunits can selectively degrade solid protein aggregates independently of ubiquitination, thereby facilitating the clearance of these aggregates (Ma et al. 2022).

All eight subunits are essential for maintaining the overall function of the entire TRiC complex and the depletion of any one of these subunits will impair its activity. It has been observed that the knockdown of CCT2/5/7 lead to impaired degradation of autophagosomes in both HeLa cells and neurons. If the complex is compromised, it results in reduced factors related to autophagosome formation, resulting in the accumulation, oligomerization and aggregation of various disease-relevant autophagy substrates, such as mutant huntington (mHTT), ATXN3, and p62 (Pavel et al. 2016). Autosomal recessive mutations in CCT4 or CCT5 can lead to sensory neuropathy,

and CCT5 expression is decreased in Alzheimer's disease (Bouhouche et al. 2006; Min et al. 2014; Pavel et al. 2016). Additionally, since TRiC is a complex structure, knockdown of one subunit may also affect the levels of other components—indeed, it has been observed that CCT2 knockdown reduces the levels of CCT7 (Pavel et al. 2016), and increased expression of CCT8 is sufficient to enhance TRiC/CCT assembly (Noormohammadi et al. 2016).

Moreover, studies have shown that both CCT3 and the apical domain of CCT1 (ApiCCT1) can reduce huntington (htt) levels in cortical neurons derived from Huntington's disease mouse models. This reduction was associated with normalized anterograde BDNF transport along with restored retrograde BDNF transport and normalized lysosomal transport. Accordingly, it appears that one primary role for this chaperone is directly regulating the aggregation involving huntingtin and other related substrates (Zhao et al. 2016).

Additionally, researchers also found that the apical domains of subunits CCT3 and CCT7 are strong inhibitors of tau aggregation, which is an important factor associated with several neurodegenerative disorders such as Alzheimer's and Parkinson's diseases (Ben-Maimon et al. 2025).
These discovery of this function provides new insights for developing therapeutic drugs and strategies for neurodegenerative diseases.

1.2 Myelin sheath

Thicker axons conduct impulse faster, but volume of the axon cannot be infinitely enlarged. Therefore, vertebrates evolved another solution for increasing action potential conduction velocity: wrapping the axon with insulation called myelin sheath (Nave & Werner 2014).

1.2.1 The function of myelin sheath

Myelin is a multilayered membranous structure that wraps around axons and is rich in lipids and myelin proteins. It consists of many layers of

membrane provided by glial support cells—Schwann cells (SCs) in the peripheral nervous system(PNS) and oligodendrocytes (OLs) in the central nervous system(CNS) (Colello & Pott 1997).

Myelin increases the speed of nerve conduction by insulating axons and thereby enabling saltatory conduction of action potentials. Furthermore, myelin protects axons and in peripheral nerves Schwann cells guide axonal regeneration. The ensheathment of axons by this multilayered glial membrane reduces the transverse capacitance and increases the transverse resistance of the axonal plasma membrane (Nave & Werner 2014). By restricting action potentials to short unmyelinated axonal segments (the nodes of Ranvier), myelin provides the structural basis for saltatory action potential propagation (Nave & Werner 2014). Numerous ion channels are present at the nodes of Ranvier, where action potentials are generated. The formation of myelin changes the conduction of action

potentials along the axon. It shifts from slower conduction along unmyelinated axons to rapid saltatory conduction between the nodes of Ranvier in myelinated axons, increasing the conduction speed by 20 to 100 times (Arancibia-Carcamo & Attwell 2014). This is crucial for fast signal transmission between neurons in the central nervous system and is important for promoting connections and rapid synchronous integration of information between different brain regions. Damage to the myelin sheath can lead to structural damage and functional impairment of the nodes of Ranvier, resulting in a decrease in action potential conduction speed.

Myelin is involved in influencing the survival of neuronal axons. Myelination significantly reduces the energy consumption of neuronal axons because action potentials are generated primarily at the nodes of Ranvier, and the ATPase consumed is only needed to restore the resting membrane potential at these nodes, which account for less than 5% of the surface

area of the entire myelinated axon (Nave 2010). More importantly, myelin provides essential energy substrates to the axon (Edgar et al. 2004; Kassmann & Nave 2008; Lappe-Siefke et al. 2003). The absence of myelin proteins can lead to degenerative damage to the axon but does not manifest as extensive myelin damage. This suggests that axonal injury may be caused by insufficient energy supply. Lactate is a substance that can be utilized by mitochondria to rapidly produce energy. It's transported to neuronal axons via Monocarboxylate Tansporter 1 (MCT1), which is abundantly expressed on myelin, to meet the energy needs of the axon (Grantham 2020). The absence of MCT1 can lead to damage to neuronal axons and loss of neurons(Grantham 2020). Similarly, it has been observed that lactate from oligodendrocytes in white matter of the central nervous system is rapidly metabolized, suggesting that myelin provides lactate to neuronal axons to meet their energy demands (Fünfschilling et al. 2012). Additionally,

oligodendrocytes can secrete neurotrophic factors such as insulin-like growth factor 1 (IGF-1), glial cell line-derived neurotrophic factor (GDNF), and nerve growth factor (NGF) (Byravan et al. 1994; Shindo et al. 2016; von Büdingen et al. 2015; Wilkins et al. 2003; Wilkins et al. 2001). Numerous pieces of evidence have confirmed that these neurotrophic factors are beneficial for neuronal survival.

Myelin affects the rapid axoplasmic transport of axons. Rapid axoplasmic transport refers to the process of transporting proteins and organelles from the neuronal cell body to the axon terminal, or vice versa (Hinckelmann et al. 2013; Millecamps & Julien 2013). In mice with a deficiency of proteolipid protein (PLP/DM20), there is a significant accumulation of membranous organelles in the optic nerve, suggesting that the axoplasmic transport dynamics in these mice are impaired. Correlation analysis has found that the dysfunction of axoplasmic transport in their

optic nerve is related to the lack of PLP/DM20 (Edgar et al. 2004). In the patients with multiple sclerosis, the levels of proteins involved in rapid axoplasmic transport are significantly decreased in the demyelinated regions of the hippocampus. These proteins include kinesin 1A, kinesin 5C, and amyloid precursor protein (APP) (Dutta et al. 2011). APP is transported from the neuronal cell body to the axon terminal via rapid axoplasmic transport, and demyelination can lead to an accumulation of APP in damaged axons.

Myelin also participates in influencing the structure and function of synapses. Damage to myelin may result in structural damage and functional impairment at synapses. The intrinsic mechanisms by which myelin affects synaptic structure and function are currently unclear. However, it's hypothesized that demyelination may influence neuronal synapses through several aspects. Neurite outgrowth inhibitor-A (Nogo-A), myelin-associated glycoprotein (MAG), and oligodendrocyte myelin

glycoprotein (OMGp) expressed on oligodendrocytes and myelin have roles in inhibiting axonal sprouting and promoting synapse formation (Baumann & Pham-Dinh 2001; Llorens et al. 2011). Impairment of myelin sheath may affect the expression of these proteins, leading to abnormalities in axonal structure and function (Llorens et al. 2011). Additionally, damage to myelin leads to disruptions in axoplasmic transport, preventing newly synthesized synaptic proteins and vesicles from being efficiently transported from the cell body to the synapse (Hinckelmann et al. 2013; Millecamps & Julien 2013). Myelin damage increases energy consumption in axons while reducing supply, resulting in insufficient energy for neurons to produce synaptic vesicles and facilitate their release (Hinckelmann et al. 2013; Millecamps & Julien 2013).

In conclusion, myelin sheath is one of the essential factors for the normal functioning of neurons in the nervous system.

1.2.2 Development of myelin in the peripheral nervous system

Prospective myelin-forming glial cells follow an intrinsic program of proliferation, migration, and differentiation, which is controlled by exogenous signals, including axonal cues (Nave & Werner 2014). As mentioned above, in the peripheral nervous system myelin is generated by myelinating SCs.

SCs originate from the neural crest of early embryos (Castelnovo et al. 2020). Under the induction of the transcription factor Sox10, neural crest cells differentiate into early SC precursors, which then further differentiate into myelinating Schwann cells. Subsequently, SCs migrate to and surround axons, establishing contacts between adjacent cells and secreting large amounts of neurotrophic factors to support axonal growth and elongation. Next, SCs proliferate and extend cytoplasmic processes to segregate axon bundles, a process known as radial sorting. After radial

sorting is completed, myelinating SCs ensheath large-diameter axons in a one-to-one manner and continue to wrap the axons in multiple concentric layers until compact myelin is formed (Kidd et al. 2013). At this stage, the SCs are referred to as myelinating SCs, and together with the axons they ensheath, they form myelinated nerve fibers. In contrast, small-diameter axons associate with non-myelinating SCs in either one-to-many or one-to-one arrangements to form Remak fibers or unmyelinated nerve fibers (Ommer et al. 2019). After myelin formation, SCs undergo remodeling to generate distinct membrane domains, each characterized by unique protein assemblies and interconnected cytoplasmic compartments (Meng et al. 2019; Salzer 2015). Myelinating SCs and axons exhibit pronounced longitudinal polarity, forming domains such as nodes, paranodes, and juxtaparanodes. Radial polarity is defined by characteristic inner and outer membrane domains located at the two ends of the cell, with compact myelin situated

between these domains. Compact myelin contains Schmidt–Lanterman incisures (SLIs), which are most abundant in large-diameter myelinated fibers. Notably, SLIs typically differentiate after the basic myelin structure has been established; they extend from the inner or outer cytoplasmic rim into the compact myelin, indicating that active loosening processes accompany the formation of the myelin lamellae (Monk et al. 2015).

1.2.3 Development of myelin in the central nervous system

Myelin in the central nervous system is generated by OLs. OLs are specialized glial cells in the CNS that originate from oligodendrocyte precursor cells (OPCs). OPCs themselves arise from earlier glial progenitors, which, while differentiating into OLs, also give rise to astrocytes. In the brain, these glial progenitors are all derived from neural stem cells (NSCs) (Shu et al. 2021). OPCs are distributed throughout the CNS and account for

approximately 5% of all CNS cells, persisting from development through adulthood and aging (Xiao & Czopka 2023). They initially arise in the ventricular zone, migrate to the adjacent subventricular zone, and subsequently undergo continuous proliferation, differentiation, and maturation to ultimately form myelin sheaths around axons.

OLs secrete various trophic cues that support axonal survival and growth, and they also provide metabolic support to axons, such as lactate (Narine and Colognato 2022; Snaidero & Simons 2017). Unlike Schwann cells (SCs) in the PNS, which myelinate only one axon, a single oligodendrocyte can myelinate multiple axons. In humans, oligodendrogenesis begins in late embryonic development and continues throughout life. In the brain's stem cell niches, NSCs differentiate into early oligodendrocyte progenitors. These newly generated OPCs migrate throughout the brain, expand in number, and populate multiple CNS regions (Dimou et al. 2008; Rowitch 2004). In adulthood, a

population of juvenile and adult OPCs maintains stable OL production across the lifespan (Hughes et al. 2013).

Upon reaching their final destinations, OPCs progress through distinct maturation stages characterized by morphological changes as well as transcriptional and proteomic remodeling. As a result of the differentiation program, immature OLs lose the ability to migrate, proliferate, and form elaborate membrane structures (Bauer et al. 2009; de Castro & Bribián 2005). Fully mature OLs produce myelin-associated proteins—such as myelin oligodendrocyte glycoprotein (MOG), myelin basic protein (MBP), proteolipid protein (PLP), and cyclic nucleotide phosphodiesterase (CNP)—which become integral components of the myelin membrane (Podbielska & Hogan 2009). Subsequently, OLs expand their membranes, interact with neuronal axons, and enwrap them (Baron & Hoekstra 2010; Podbielska & Hogan 2009).

The final step of myelination is myelin compaction. During this process, the intracellular and extracellular leaflets of adjacent myelin membranes are drawn tightly together by myelin proteins. MBP, a key protein in myelin formation, mediates the compaction of intracellular leaflets by adhering the cytoplasmic surfaces of myelin membranes, whereas PLP is responsible for compacting the extracellular leaflets. Through lipid-rich membrane compaction and tight lamellar wrapping, mature myelin ultimately fulfills its function as an electrical insulator for axonal signal conduction (Kang & Yao 2022).

In the mammalian cerebral cortex, OPC development and myelination occur throughout nearly the entire lifespan (Hughes et al. 2018). From birth to middle age, OPCs continuously generate new myelinating OLs in the somatosensory cortex (Hill et al. 2018; Hughes et al. 2018). Proper OPC development is essential for the formation of functional myelin.

1.3 Microtubules – a main component of the cytoskeleton

To grow, divide, and adapt to fluctuating conditions, all cells require the capacity to continually reorganize their internal components. These spatial and mechanical functions are supported by an intricate system of filaments collectively referred to as the cytoskeleton. Eukaryotes have the most complex cytoskeletons, comprising three cytoskeletal polymers—actin filaments, intermediate filaments, and microtubules—acted on by three families of motor proteins (myosin, kinesin, and dynein) (Pollard & Goldman 2018). Each type of filament has distinct mechanical properties, dynamics, and biological roles, but all share certain fundamental features.

1.3.1 The structure of microtubules

Microtubules are essential components of cytoskeleton that help determine the shape of a cell (Avila 1992). They're hollow, elliptical

structures composed of 13 protofilaments arranged in a radial array by the centrosome (Chaaban & Brouhard 2017; Nekooki-Machida & Hagiwara 2020). Each protofilament is formed by the vertical polymerization of α- and β-tubulin, when subsequently associate laterally to assemble into the microtubule(Chaaban & Brouhard 2017; Nekooki-Machida & Hagiwara 2020). Both α- and β-tubulin contain a GTP-binding site. When α- and β-tubulin form a heterodimer, the GTP-binding site on α-tubulin becomes buried within the dimer, rendering the bound GTP nonhydrolyzable and nonexchangeable; this site is therefore referred to as the nonexchangeable (N) site (Howard & Hyman 2007). The α- and β-tubulin share approximately 50% sequence homology at the amino acid level, and each has a molecular weight of about 50 kDa (Desai & Mitchison 1997).

Microtubules exhibit inherent polarity, possessing two structurally and functionally

distinct ends - the plus end and the minus end - which is crucial for their biological function (Akhmanova & Hoogenraad 2015; Walker et al. 1988). Tubulin dimers polymerize in a head-to-tail manner, with the β-subunit of one dimer contacting the α-subunit of the next (Walker et al. 1988). Consequently, each protofilament exposes α-tubulin at one end and β-tubulin at the other, defining the minus and plus ends, respectively (Akhmanova & Hoogenraad 2015). Protofilaments align in parallel with uniform polarity such that, within a microtubule, the plus end exclusively exposes β-tubulin, whereas the minus end exposes only α-tubulin (Akhmanova & Hoogenraad 2015). Although polymerization can occur at both ends, elongation is significantly faster at the plus end (Akhmanova & Hoogenraad 2015).

1.3.2 The function of microtubules

Microtubules exhibit dynamic polymerization and depolymerization properties and play essential roles in maintaining cell morphology,

cell division, signal transduction, and intracellular transport (Avila 1992; Nogales 2000). Under physiological conditions, cellular architecture, organelle positioning, and organelle function all depend on the stability of the microtubule network (Avila 1992; Nogales 2000).

Microtubules assist in maintaining cell morphology. As a major component of the cytoskeleton, microtubules provide structural support for cells, maintain asymmetric cell shapes and structural stability, and help establish cellular polarity and directional orientation(Avila 1992; Nogales 2000). For example, in neurons, microtubules are arranged along the longitudinal axis of axons and dendrites, supporting these elongated structures. In epithelial cells, microtubules help maintain the flattened cellular morphology. In addition, microtubules also play a crucial role in organizing the intracellular organelles(Avila 1992; Nogales 2000). Mitochondria are distributed in association with microtubules;

free ribosomes are attached at the intersections of microtubules and microfilaments; and microtubules enable the endoplasmic reticulum to extend throughout the cytoplasm while positioning the Golgi apparatus centrally near the nucleus, in proximity to the centrosome(Avila 1992; Nogales 2000).

Microtubules play an essential structural role in eukaryotic cilia and flagella. These organelles are ubiquitous microtubule-based eukaryotic organelles that project from the cell to generate motility or function in cellular signaling (Klena & Pigino 2022). Dynein motors act on the microtubule bundles that run along the length of the cilium or flagellum, enabling these organelles to bend and generate force for functions such as motility, propulsion, and the transport of extracellular materials. Cilia and flagella are specialized organelles widely distributed among eukaryotic organisms. The core structure of motile cilia, the axoneme, consists of a pair of microtubule singlets termed the central pair complex (CPC) and nine

peripherally positioned doublet microtubules (DMTs), which form a ‘9+2′ architecture (Klena & Pigino 2022; Xia et al. 2025). Each DMT consisting of an A-tubule and a B-tubule. The A-tubule is a complete microtubule comprising 13 protofilaments, whereas the B-tubule is an incomplete microtubule containing only 10 protofilaments, and two junctions connect the A- and B-tubules, termed the outer junction (OJ) and the inner junction (IJ).

Microtubules play a central role in intracellular transport, serving as “tracks” along which motor protein - including kinesin and dynein - which travel along microtubules to deliver vesicles, organelles (such as mitochondria and ribosomes), and various macromolecules (Goodson & Jonasson 2018). In neurons, for example, proteins and membrane components synthesized in the soma are transported along axonal microtubules to the axon terminals. A key function of the neuronal microtubule cytoskeleton is therefore to support long-range, motor-driven transport. Moreover, microtubule

properties, including post-translational modifications (PTMs) can affect motor protein activity (Yogev et al. 2016) Studies have shown that axonal transport requires metabolic energy and depends on an intact microtubule network (Millecamps & Julien 2013; Niwa et al. 2013; Yogev et al. 2016).

The functions of microtubules are closely linked to their dynamic assembly and disassembly properties, which allow them to rapidly respond to intracellular and extracellular signals and to adapt to various physiological demands of the cell.

1.3.3 Microtubule dynamics

When an α-tubulin and a β-tubulin subunit are tightly bound together, they form the fundamental “building block” of a microtubule. Thousands of these blocks assemble to form a hollow tubular structure approximately 25 nm in diameter. Importantly, these building blocks are not static, instead, microtubules constantly switch between phases of growth and

shrinkage. The addition of new subunits typically occurs at the more dynamic plus end, whereas the opposite end is relatively stable and is referred to as the minus end (Akhmanova & Hoogenraad 2015). Microtubule growth relies on a key chemical condition: the energy stored in GTP. Because of the unique structural properties of tubulin dimers, the GTP bound to β-tubulin is hydrolyzable. This hydrolysis occurs very slowly when tubulin dimers are free in solution, but it accelerates once the dimers are incorporated into the microtubule, and tubulin is therefore considered a GTPase (Alushin et al., 2014; Bowne-Anderson et al., 2015; Bowne-Anderson et al., 2013). After GTP hydrolysis, the inorganic phosphate is released, while GDP remains bound to β-tubulin within the microtubule lattice. Based on the hydrolysis state, tubulin dimers can be classified into two forms: the GTP-bound T-form and the GDP-bound D-form (Bowne-Anderson et al. 2013). Under physiological conditions, T-form dimers

preferentially polymerize, whereas D-form dimers tend to depolymerize.

Because GTP-bound tubulin is incorporated at the microtubule end, it is thought that a “GTP cap” composed of T-form tubulin exists at the plus end, protecting the microtubule from depolymerization. When GTP hydrolysis reaches the microtubule end, the microtubule undergoes rapid depolymerization and shortening—a transition known as catastrophe. Incorporation of new GTP-bound tubulin at the microtubule end can reestablish the protective cap and halt shrinkage, a process referred to as rescue (Bowne-Anderson et al. 2015). The growth rate, shrinkage rate, catastrophe frequency, and rescue frequency constitute the four fundamental parameters of microtubule dynamics. Among a population of microtubules, some ends are in the T-form state while others are in the D-form state at any given time, and the relative proportion of T-form versus D-form ends is determined by the rate of GTP hydrolysis and the concentration of free tubulin

dimers (Bowne-Anderson et al. 2015). Microtubules are characteristically defined by a constant cycling between growing and shrinking referred to as dynamic instability (Logan & Menko 2019; Mitchison & Kirschner 1984). At the plus end of microtubules, the growth rate is faster than the shrinkage rate because of the exist of the GTP cap. However, it's opposite at the minus end of microtubules, which leads to the total length of microtubules remain unchangeable and the tubulin dimers move from the plus end to the minus end. This phenomenon is called "treadmill" of microtubules (Wang et al. 2016).

1.3.4 Microtubule-binding proteins (MTBPs)

It's observed that microtubule dynamics show numerous differences between intra- and extracellular environments (Kinoshita et al. 2001; Zanic et al. 2013). Microtubules tend to show stronger ability to polymerization intracellular. At similar concentration of tubulin dimers, the intracellular growth rates typically

range from 10 to 15 μm per minute, whereas the extracellular growth rates are about 1.5 μm per minute (Kinoshita et al. 2001; Srayko et al. 2005; Zanic et al. 2013). Moreover, microtubules polymerized extracellularly present a higher catastrophe frequency and a lower rescue frequency (Al-Bassam et al. 2010). The reason of these differences is that the microtubule dynamics in cells is tightly regulated by many microtubule-binding proteins (MTBPs) (Al-Bassam et al. 2010).

1.3.4.1 Microtubule-associated proteins (MAPs)

MAPs, including tau, MAP2 and MAP4 are a group of proteins that bind to microtubules (Dehmelt & Halpain 2005; Goodson & Jonasson 2018). The Tau/MAP2/MAP4 family has the feature of C-terminal microtubule binding repeats, a central proline-rich region and an N-terminal projection domain (Cario & Berger 2023). Their primary functions include promoting microtubule assembly, enhancing

structural stability, mediating intracellular transport, and regulating microtubule dynamics. They account for about 10–15% of the microtubule structure and play essential roles in cell division and neuronal development. Tau and MAP2 are neuronal microtubule stabilizers that are localized to axons and dendrites, respectively, and MAP4 is expressed in most tissues (Goodson & Jonasson 2018). Tau is related to some neurodegenerative diseases, collectively known as Tauopathies, including Progressive Alzheimer's Disease (AD), Frontotemporal Dementia (FTD) and Supranuclear Palsy (PSP) (Cario & Berger 2023). In patients with Alzheimer's disease, tau proteins exhibit abnormally higher levels of phosphorylation, causing them to detach from microtubule and gather in the brain, which leads to a loss of their normal biological functions and reduced affinity for microtubules (van de Willige et al. 2016). As a result, neurofibrillary tangles (NFTs) are formed. MAP2/Tau family members are naturally

unfolded proteins. They will form specific conformations while binding to their targets (microtubules, F-actin and potentially other molecules) (Dehmelt & Halpain 2005). It's acknowledged that the occurrence of Tauopathies is because of the loss of microtubule stability in the axon (Cario & Berger 2023). The interaction of Tau and microtubule will be impaired by the mutation related to Tauopathies or abnormal PTMs (Dehmelt & Halpain 2005).

1.3.4.2 Plus-end tracking proteins (+TIPs)

A part of microtubule-binding proteins can track the growing plus ends of microtubules through various mechanisms, which is called plus-end tracking proteins (+TIPs). +TIPs can be claasified into three catagories: end-binding proteins (EBs), EB-dependent +TIPs and EB-independent +TIPs, and EBs are the most abundant +TIPs (van de Willige et al. 2016). The EBs family includes EB1, EB2, and EB3, and all of them can combine with the plus end

of microtubules. However, they differ in the affinity to the end of microtubules and in their phosphorylation status (Komarova et al. 2009; van de Willige et al. 2016). EB1 and EB2 are expressed widely in various cells, while EB3 is highly expressed in brain and muscle cells (Komarova et al. 2009; Su & Qi 2001; van de Willige et al. 2016). Studies have shown that during the neuronal development, the expression of EB1 decreases , whereas the expression of EB1 increases (Jaworski et al. 2009; van de Willige et al. 2016). In neuroblastoma cells, axon elongation and the expression of EB occur simultaneously (Morrison et al. 2002). Loss of EB1 impairs axon growth and causes microtubule disorganization in *Drosophila*, however, it doesn't lead to loss of microtubule loss (Alves-Silva et al. 2012). Other studies have also highlighted a role for EB1 in axonogenesis and suggest that EB proteins may play distinct roles in neurite formation (Jiménez-Mateos et al. 2005). EB1 and EB3 promote neurite outgrowth,

whereas EB2 appears to have a negative effect (Arens et al. 2013) EB3 has been shown to be closely associated with neuritogenesis through its involvement in the interactions between actin and microtubule (Geraldo et al. 2008). This finding indicates that EB family play crucial roles in controlling neuronal morphogenesis.

1.3.4.3 Motor proteins

Motor proteins are utilized to transport cargos and execute various other functions in cells (Arriagada 2017; Dodding & Way 2011; Döhner et al. 2005). They can be divided into three catagories including dynein, kinesin and myosin. The main difference among them is that dynein and kinesin use microtubules as “tracks”, while myosin use actin filaments as “tracks”. Both kinesin and dynein are composed of two identical heavy chains, which make up two large globular head domains, and a variable number of intermediate and light chains. The globular head domains specifically bind to microtubules, while the tail stably

interacts with cellular components such as vesicles and organelles. Kinesins generally deliver organelles, vesicles and newly synthesized proteins towards the microtubule plus end (anterograde transport), whereas dyneins carry endocytosed vesicles and recycle damaged or misfolded proteins and organelles from distal cellular regions in the opposite direction (retrograde transport) (Yildiz 2025).

Kinesins are microtubule-dependent motor proteins with a highly conserved motor domain. Based on the position of the motor domain, kinesins are classified into N-kinesins (the motor domain located at the N terminus), M-kinesins (the motor domain located in the middle of the peptide chain) and C-kinesins (the motor domain located at the C terminus) (Hirokawa et al. 2009; Yildiz 2025). N-kinesins drive anterograde transport by moving cargo toward the microtubule plus end. M-kinesins lack directional bias and instead remove tubulin subunits from microtubule ends, whereas C-

kinesins mediate retrograde transport toward the minus end (Yildiz & Zhao 2023).

Dyneins are minus end-directed motor proteins composed of multiple AAA+ modules, forming a large multimeric complex with a hexameric ATPase ring (Yildiz & Zhao 2023). Dyneins generate force through ATP hydrolysis to drive cargo transport toward the microtubule minus end.

1.4 Axonal transport

Axonal transport, also called axoplasmic transport or axoplasmic flow, is the cellular process responsible for moving lipids, synaptic vesicles, proteins, mitochondria and other organelles to and from a neuron's cell body, through the cytoplasm of its axon called the axoplasm (Sabry et al. 1995). Axonal transport is a key mechanism by which neurons achieve directional movement of cargos between the cell body and the axon terminal through the cytoskeleton. It includes anterograde transport (toward the axon terminal) and retrograde

transport (toward the cell body). This process is carried out by motor proteins, including kinesin and dynein, which move along microtubules.

1.4.1 Anterograde transport

Anterograde axonal transport refers to the kinesin-mediated movement of cargo from the cell body toward the axon terminal, supplying proteins and lipids to the nerve terminal and meeting local energy demands.

1.4.2 Retrograde transport

Retrograde axonal transport is mediated by dynein and involves the movement of cargo from the axon terminal back to the cell body. This process contributes to the clearance of misfolded or aggregated proteins and the intracellular transport of distal trophic signals to the cell body.

Studies have shown that neurons show specifically sensitivity to the disorder of the retrograde motor proteins (Perlson et al. 2010). Alterations of dynein and dynactin can also

impair retrograde axonal transport and then result in neurodegenerative diseases (Ström et al. 2008). Previous studies have reported that the impairment of retrograde axonal transport have been observed in the mouse model $SOD1^{G93A}$ (mSOD1) of Amyotrophic lateral sclerosis (ALS) (Perlson et al. 2009; Ström et al. 2008). The co-localization of dynein and mutant SOD has been detected in the axons of the ALS mouse model (Ligon et al. 2005; Ström et al. 2008).

2 Research Objective

Mutations in *CCT* genes are linked to neurological diseases in humans. CCT3 is an essential subunit of TRiC/CCT, a chaperonin responsible for folding actin and tubulin, two essential components of the cytoskeleton that are necessary for cellular trafficking and dynamics. A CCT3 loss-of-function zebrafish model that has recently been established in the

lab showed smaller eyes and brain, as well as reduced myelin formation.

First, I aimed at quantifying the reduced motor response upon stimulation in *cct3* mutant larvae and to demonstrate that the observed phenotypes were indeed due to loss of cct3 function. To do so, I stimulated individual larvae mechanically and determined their response rate under a stereomicroscope. Furthermore, I generated compound heterozygous mutants and microinjected wildtype *cct3* mRNA into *cct3* mutant embryos followed by assessing the morphological development.

Next, I aimed at determining how the loss of cct3 affects cytoskeleton in neurons, i.e. actin and microtubules and axonal transport of organelles. To address these, I determined amounts and distribution of actin and tubulin by performing Western blots, stainings and/or immunolabelings. I also combined the *cct3* mutant allele with different transgenic lines that fluorescently label subcellular organelles in

neurons and performed live imaging on a spinning disc confocal microscope.

To determine the role of cct3 in neuromuscular junction formation, I performed stainings of neuromuscular junctions at different time points of development. To assess Schwann cell development and survival during peripheral nerve myelination. I combined the *cct3* mutant allele with different transgenic lines that fluorescently label neurons and Schwann cells and performed live imaging on a spinning disc confocal microscope. To determine whether the observed reduction of Schwann cells was due to apoptotic cell death, I performed immunolabling of activated Caspase 3.

3 Materials and Methods

3.1 Materials

3.1.1 Zebrafish lines

All zebrafish lines used within this project are shown in this section (Table 1).

Table 1: Wild type (WT) mutant and transgenic zebrafish lines used in this thesis.

Zebrafish line	ZFIN reference
Tüpfel long fin (TL)	(Baumann and Pham-Dinh, 2001; Llorens et al., 2011)
AB	(Hinckelmann et al., 2013; Millecamps and Julien, 2013)
cct3$^{p.G54Vfs*57}$ *(cct3-1)*	CRISPR/Cas9-generated
cct3$^{p.Gly55Serfs*57}$ *(cct3-2)*	CRISPR/Cas9-generated
Tg(*mnx1:Gal4*)	-
Tg(UAS:lifeact-GFP-v2A-EB3-RFP)^{p412}	-
Tg(*UAS:mito-mCherry*)	-
Tg(Xla.Tubb:DsRed)^{zf148}	-
Tg(*UAS:EGFP-rab7a*)	-

Zebrafish line	ZFIN reference
Tg(sox10:nlsEOS)^{w18Tg}	ZDB-TGCONSTRCT-081023-2

3.1.1.1 Wildtype fishline

These zebrafish were used to generate CRISPR/Cas9 mutants and transgenic lines.

3.1.1.2 Mutants fishlines

By using the CRISPR/Cas9 method deletions in the target sequence in exon 4 of cct3 were generated. Loss-of-function alleles of cct3 were generated using CIRSPR/Cas9 with the target sequence: 5'-GGTCATGACGATACCACCCATGG-3' located in exon 4 of the cct3 gene as previously described. Single guide RNAs were cloned using the DR274 plasmid. The established zebrafish line was further characterized by sequencing, revealing a 4 bp deletion in exon 4 (NM173250.1:c.161_164del), causing a frameshift mutation. This mutation resulted in the substitution of glycine (G) with valine (V) at position 54, leading to a premature stop codon

at position 57 (cct3p.G54Vfs*4). Additionally, a second zebrafish line harboring a 4 bp deletion in exon 4 (NM173250.1:c.163_166del) leading to a frameshift mutation was generated. In this line, the mutation caused a substitution of glycine (G) with serine (S) in position 55, resulting in a premature stop codon at position 57 (cct3p.G55Sfs*3).

3.1.1.3 Transgenic fishlines

To drive Gal4 expression in motor neurons, *Tg*(*mnx1:Gal4*) zebrafish line was generated using I-SceI (meganuclease). To label F-actin and microtubules simultaneously, *Tg*(UAS:lifeact-GFP-v2A-EB3-RFP) zebrafish line was generated using Tol2 transgenesis, expressing GFP-tagged F-actin-binding lifeact76 and RFP-tagged human EB3, both separated by self-cleaving viral 2A peptide. For visualization of mitochondria and endosomes, two new fish lines, *Tg*(*UAS:mito-mCherry*) and *Tg*(*UAS: EGFP-rab7a*) were generated. Both lines were combined with *Tg(mnx1:Gal4)* to label mitochondria and Rab7^{+} endosomes in

mnx1-expressing motor neurons. Neural crest-derived cells, including Schwann cells were labeled using the *Tg(sox10:mRFP)*^{vu234} (RFP-labelling of membranes), and *Tg(sox10:nlsEOS)*^{w18Tg} (nuclear labeling with EOS).

3.1.2 Oligonucleotides (Primers)

The Primers used for Genotyping of cct3 are shown in Table 2.

Table 2: dCAPS oligonucleotides used for genotyping.

Allele	Orientation	Length [nt]	Sequence [5'-3']
cct3-1	cct3-1$^{dCAPS-fw}$	21	CAGATGCTGCTGGATCCGACGG
	cct3-1$^{dCAPS-rev}$	22	GGATGCTGGACCTGGATCTAAA
cct3-2	cct3-2$^{dCAPS-fw}$	22	GATGCTGCTGGATCGAATGGGT
	cct3-2$^{dCAPS-rev}$	24	GGATGCTGGACCTGGATCTAAAGT

The ordered primers were diluted into a FRW primer stock using 15 µL of each 100 mM primer (forward and reverse) and 270 µL

nuclease-free water to achieve a final concentration of 3.75 µM.

Table 3: Additional primers

Gene	Orientation	Sequence	Function
M13	forward	GTAAAACGACGGCCAG	Sequencing of pCR™ 2.1-TOPO™ TA-Vector and pCS2+
M13	reverse	CAGGAAACAGCTATGAC	Sequencing of pCR™ 2.1-TOPO™ TA-Vector
SP6	forward	ATTTAGGTGACACTATAG	Sequencing of pCS2+

3.1.3 Buffers and solutions

All buffers and solutions used for this work are shown in Table 4. Ordered commercial buffers are shown in Table 5.

Table 4: Buffers and solutions with recipe

Buffer / solution	Composition	Utilization
Bleaching solution	375 µL sodium hypochlorite solution (5-10% Cl) 1.5 L of E3 buffer	Bleach

Buffer / solution	Composition	Utilization
Green PCR mix	18,6 ml ddH20 6,48 ml 5 x Green GoTaq® Flexi buffer 1,3 ml dNTPs [5mM each] 2,6 ml $MgCl_2$	PCR
KCl	0.1 M KCl (filtered)	Microinjection
Lysis buffer	1x RAPD 0.3% Tween-20 0.3% NP40 100 µg/ml Proteinase K	DNA extraction
P1 (Resuspension Buffer) with RNase	500 mL Buffer P1 (Resuspension Buffer) 100 µg/mL RNase A	Miniprep
PBS / PBST (1x)	0.14 M NaCl 10 mM Na_2HPO_4 2.8 mM KH_2PO_4 2.7 mM KCl (for PBST: 0,1% Tween-20 was added)	Immunostaining/WB
TBE, pH 8.3 (0,5x)	0,44 M Tris base	Gel electrophoresis

Buffer / solution	Composition	Utilization
	0,44 M boric acid 1 mM EDTA pH 8.0	
Tricaine	0.01% Tricaine	Anesthesia of larvae and adult fish Immunostaining
Blocking Solution	0.2% BSA 0.1% Tween-20 1%NGS	Immunostaining

Table 5: Commercial buffers and solutions

Buffer	Manufacturer	Reference
Buffer P1 (Resuspension Buffer)	Qiagen (Venlo, Netherlands)	#19051
Buffer P2 (Lysis Buffer)	Qiagen (Venlo, Netherlands)	#19052
Buffer P3 (Neutralization Buffer)	Qiagen (Venlo, Netherlands)	#19053
rCutSmart™ (10x)	New England Biolabs (Ipswich, MA, USA)	#B6004S

3.1.4 Media

All media used for this work are shown in Table 6. LB agar and LB medium were autoclaved

before using and mixed with antibiotics after cooling. Either 100 µg/mL of Ampicillin or 50 µg/mL of Kanamycin were used.

Table 6: Used media with information regarding their composition or manufacturer.

Media	Composition / Manufacturer	Utilization
E3 buffer	5 mM NaCl 0.17 mM KCl 0.33 mM $CaCl_2$	Raising embryos and larvae until day 5
LB agar	1.5% Bacto Agar 1% Bacto Trypton 0.5% Yeast extract 17.25 mM NaCl in ddH_2O Ampicillin 100 µg/ml or Kanamycin 50 µg/ml	cultivation of bacteria
LB medium	1% Bacto Trypton 0.5% Yeast 17.25 mM NaCl in ddH_2O Ampicillin 100µg/ml or Kanamycin 50µg/ml	cultivation of bacteria
SOC medium	Invitrogen (Carlsbad, USA), 15544034	Transformation

3.1.5 Kits

All kits used for this work are shown in Table 7.

Table7: Commercial kits

Kits	Manufacturer	Reference
GoTaq® DNA Polymerase (with buffers)	Promega (Madison, USA)	#M3001
MEGAclear™ Kit	Invitrogen (Carlsbad, USA)	#AM1908
MEGAshortscript™ Kit	Invitrogen (Carlsbad, USA)	#AM1354
NucleoBond® Xtra Midi	Macherey-Nagel (Düren, Germany)	#740410
QIAquick Gel Extraction Kit	Qiagen (Venlo, Netherlands)	#28706X4
QIAquick PCR Purification Kit	Qiagen (Venlo, Netherlands)	#28104
*Pfu*Turbo DNA Polymerase (with buffers)	Agilent Technologies (Santa Clara, USA)	#600250
RNeasy® Mini Kit	Qiagen (Venlo, Netherlands)	#74104
TOPO™ TA Cloning™ Kit	Invitrogen (Carlsbad, USA)	#K202040

Kits	Manufacturer	Reference
SP6 mMESSAGE mMACHINE	Invitrogen (Carlsbad, USA)	#AM1340

3.1.6 Enzymes

All restriction enzymes and other enzymes for this work are shown in Table 8 and Table 9. All restriction enzymes were obtained from New England Biolabs (NEB) [Ipswich, MA, USA].

Table 8: Restriction enzymes

Enzymes	$T_{Incubation}$ [°C]	$T_{Inactivation}$ [°C]	Reference
EcoRI	37	65	#R0101
DrdI	37	65	#R0530
XmnI	37	65	#R0194

Table 9: Other enzymes

Enzymes	Manufacturer	Reference
Pronase	Roche (Basel, Switzerland)	#10165921001
RNase A	Qiagen (Venlo, Netherlands)	#1007885

3.1.7 Antibodies

All antibodies used for this work are shown Table 10.

Table 10: Antibodies

Antibody	Supplier	Utilization
Bungarotoxin (AF 488 conjugate)	Invitrogen (Carlsbad, USA), #B13422	Immunostaining
α-Znp-1 (synaptogamin-2)	ZIRC (Eugene, USA), #ZDB-ATB-081002-25	Immunostaining
anti-Mouse IgG2a (AF 594 conjugated)	Invitrogen (Carlsbad, USA), #A-21135	Immunostaining
anti-vinculin primary antibody	Merck Millipore, #MAB3574	Immunostaining
TRITC-conjugated phalloidin	Merck Millipore, #90228	Immunostaining
anti-acetylated tubulin primary antibody	Sigma-Aldrich, #T679	
anti-mouse IgG2b secondary antibody Alexa Fluor™ 488 conjugate	Invitrogen (Carlsbad, USA), #A-21141	Immunostaining
anti-Polyglutamylation Modification mAb	Adipogen; #AG-20B-0020-C100	Immunostaining
anti-mouse IgG1 secondary antibody Alexa Fluor™ 594 conjugate	Invitrogen (Carlsbad, USA), #A-21125	Immunostaining

Antibody	Supplier	Utilization
TCP-1 γ antibody	Santa Cruz; #sc-271336	Western Blot
anti-actin	Abcam; #ab6276	Western Blot
anti-α-Tubulin	Sigma-Aldrich; #T5168	Western Blot
anti-GAPDH	Abcam, EPR16891	Western Blot
HRP-conjugated secondary antibodies(anti-mouse and anti-rabbit)	Invitrogen; #32430 Invitrogen; #31460	Western Blot

3.1.8 Bacteria

Competent cells were used One Shot™ TOP10 Chemically Competent E. coli from Invitrogen by Thermo Fisher Scientific (Waltham, MA, USA) (#C404010).

3.1.9 General Reagents

All General reagents and chemicals are listed in Table 11.

Table 11: General reagents and chemicals

Chemical	Manufacturer	Reference
Agarose	Biozym	#840004
Ampicillin	Sigma-Aldrich	#A9518

Chemical	Manufacturer	Reference
Calcium chloride ($CaCl_2$)	Sigma-Aldrich	#102382.0500
Collagenase	Sigma-Aldrich	#C9891
Dimethyl sulfoxide (DMSO)	Sigma-Aldrich	#317275
DNA loading dye purple (6x)	Biolab	#B7024A
Ethanol p.a.	VWR	#100989.1011
GelRed® (10,000x)	Biotium	#41003
GeneRuler DNA ladder	Invitrogen	#SM0331
Isopropanol p.a.	VWR	#109634.2511
Low melting agarose	Biozym	#840001
Magnesium chloride ($MgCl_2$)	ROTH	#105833.1000
Methanol p.a.	Hpneywell	#104873
Monopotassium phosphate (KH_2PO_4)	Sigma-Aldrich	#104877.1000
Sodium Chloride (NaCl)	ROTH	#9265.1
Sodium hydrogen carbonat	Sigma-Aldrich	#S5761
Paraformaldehyde (PFA)	ROTH	#P6148
Phenol red	Sigma-Aldrich	#P0290
Potassium Chloride (KCl)	Sigma-Aldrich	#104936.1000
Sodium bicarbonate	Sigma-Aldrich	#S6014

Chemical	Manufacturer	Reference
Sodium hypochloride solution	ROTH	#6846.1
Tricaine	Sigma-Aldrich	#A5040
Triton X-100	Sigma-Aldrich	#X100
Tween-20	Sigma-Aldrich	#822184.0500
Vectashield	Biozol	#ZJ0401
Bovine serum albumin (BSA)	Invitrogen	#37525
Gylcerol	Sigma-Aldrich	#G2025
Normal goat serum (NGS)	Abcam	# ab7481
SeaPlaque™ (low melting) agarose	Lonza	#50100
Tris ($NH_2C(CH_2OH)_3$)	Sigma Aldrich	#T6066
Trizol	Invitrogen	#15596018
Protease inhibitor	Sigma Aldrich	#P8340
Blocking Reagent	Roche	#1096176
SuperSignal™ West Femto Maximum Sensitivity Substrate	Invitrogen	#34095

3.1.10 Consumables

All consumables used for this work are listed in Table 12.

Table 12: Used consumables with information regarding the manufacturer.

Consumables	Manufacturer
0.2-mL PCR tubes	Biozym
24-/48-well plates	TPP
96-Well PCR plate	Biozym
Glass bottom microwell dishes	MatTek
Glass capillaries	WPI
Glass multi-well plates	Pyrex
Centrifuge tubes 15 mL	Sarstedt
Centrifuge tubes 50 mL	Sarstedt
Cover slip	Epredia
Microcentrifuge tubes 1.5 mL	Sarstedt
Microcentrifuge tubes 2.0 mL	TubeOne
Microscope slide	R. Langenbrinck GmbH
Nail Polish	Maybelline
Pasteur pipettes	-
Petri dishes (10 mm)	Sarstedt
Pipette tips	Eppendorf
Pipette filter tips	Eppendorf
Scalpels	Feather
Sterile culture tubes 12 mL	ROTH

3.1.11 Software and Devices

All software used in this work are listed in Table 13.

Table 13: Used software and devices

Software	Provider
FIJI / ImageJ (Version 2.9.0/1.53.t)	Open source (www.fiji.sc)
Microsoft Office for Mac (Version 16.103)	Microsoft (Redmond, USA)
SnapGene Viewer 6.1	Dotmatics (Boston, USA)
VisiView® software	Visitron Systems (Puchheim, Germany)
iBright™ FL1500 Imaging System	Invitrogen
Ti Eclipse Microscope	Nikon (Tokyo, Japan)

3.1.12 Artificial Intelligence/ChatGPT

ChatGPT was used for language correction and German translation, not text-writing.

3.2 Methods

3.2.1 Zebrafish related methods

All procedures were performed according to the German 'Tierschutz-Versuchstierverordnung (TierSchVersV)'. Husbandry of zebrafish was approved by the 'Landesamt für Natur, Umwelt und Verbraucherschutz Nordrhein-Westfalen (LANUV)' ('Haltungsbewilligung' 39.2.60.06.04). The generation of mutant lines and transgenic lines as well as breeding of

those lines were also permitted by the LANUV ('Generierungsrahmenantrag' 81-02.04.2021.A033 and 'Zuchtrahmenantrag' 81-02.04.2021.A304). Fin-clipping of zebrafish ordered from the European Zebrafish Resource Center (EZRC) was authorized in a permit called 'Schwanzflossenbiopsien' (81-02.05.40.21.001).

3.2.1.1 Zebrafish Housing and Husbandry

Zebrafish embryos and larvae are raised in an incubator in the Uniklinik RWTH Aachen (Floor -2, Corridor 22, Room 4) at 28°C until day 5. If embryos were meant to be raised to adulthood, embryos need to be bleached at approximately 24 hpf. 5 bowls were filled with 25 mL of 60x E3 medium. 375 µL of the Bleach stock solution, sodium hypochlorite by Carl Roth (Karlsruhe, Germany) (#6846.1), was added into bowl 1 and 3. All bowls were filled with VE-water up to 1,5 L. The washing solutions are now in the following order: bleach solution, tap water, bleach solution, tap water and tap water. Then

I transferred all embryos of one clutch into one strainer. Six strainers can be bleached simultaneously. Then the embryos were incubated in the bowls one after the other for exactly five minutes each. After the last bowl I transferred the embryos into a new dish containing 12 µl of 30mg/mL pronase from Roche (Basel, Switzerland) (#10165921001). The embryos are raised in the 28°C incubator again. The next day the pronase needs to be removed by changing the E3 medium. Then they are transferred into a 3.3 L Aqua Box (by AquaSchwarz) in the fish room on day 5. Water temperature was set to 26 ± 2 °C. Conductivity ranged between 150-1700 µS/cm, while a pH of 7 to 8 was deemed acceptable. Until 12 dpf there is no waterflow into the box and the larvae get fed with 50 mL *Paramecia* twice a day. At day 12-15 dpf they get fed with 50 mL *Paramecia* and *Artemia*. From day 15 until three months the fish are being fed with *Artemia* thrice a day. After three months, they get fed with *Artemia* in the morning and with dry food at

noon. *Paramecia* are raised in 5 L plastic canister with 4 mL of wheat germs and 6 mL of brewer's yeast. 18 mg of *Artemia* eggs (Sanders Great Salt Lake Artemia (South Ogden, UT, USA)) are raised in 12 L tap water with 150 g sea salt in a funnel with an aerator for the day after next. Because of live feeds like *Artemia* the fish can catch the prey as they would in nature. Once the fish are genotyped (around 3 months old), they get transferred into 9.8 L glass tanks. The system water is changed daily and includes distilled water with 22 g Coral Pro Salt from Red Sea (Houston, TX, USA), 11 g Sodium bicarbonate from Sigma-Aldrich (St. Louis, MO, USA) (#S6014) and 5.6 g Calcium sulfate dihydrate from VWR International (Radnor, PA, USA) (#10101-41-4). In the fish room is a dark-light cycle installed, so 14 hours a day there is light and 10 hours darkness. Once a week we test the water for nitrite with the test kit from JBL (#2537000). Normally the value is below 0.5 mg/mL. In the fish room are two different zones, the main and the

quarantine. Purchased fish are only allowed in the quarantine because of a possible spread of potential pathogens. Only the fish born in the facility and bleached as embryos are allowed to be raised in the main system.

3.2.1.2 Mating procedure

Zebrafish matings were set up in the afternoon. A female and a male were placed in a 1 L breeding tank with an internal tank to keep the fish from eating their eggs. The fish produce embryos shortly after sunrise which is simulated by the dark-light-cycle. If it was necessary to time the mating, I kept the fish separated by a divider overnight, removed the divider when necessary and collected the eggs right away.

3.2.1.3 Fin biopsies

For genotyping using PCRs on DNA obtained from individual fish, caudal fin biopsies were taken. A single fish was transferred from its tank into a separate container to be anesthetized in

approximately 500 mL of 0.01% tricaine. Once anesthetized, it was transferred to a Petri dish using a sieve. A small part of the caudal fin was cut off with a scalpel and placed in a 0.2-mL PCR tube containing methanol. After the fin biopsy was taken, the fish was immediately transferred to a recovery tank containing 0.5 L of water to wake up from anesthesia. After fin-clipping, the fish were stored in separate tanks without water connection. Normally, the genotype was determined within 48 h.

3.2.1.4 Live imaging and time-lapse microscopy

Live embryos and larvae aged between 1-5 dpf were mounted in 0.8% low melt agarose in E3 containing 0.022% tricaine onto Nunc™ glass bottom dishes (12 mm). To prevent the agarose from drying out, it was covered with 0.022% tricaine in E3. Live imaging was performed with a spinning disk confocal microscope (Nikon Eclipse TI) at a 60x lateral magnification using an Olympus (U Plan S Apo) objective lens and

water as immersion solution. GFP was excited with a 488 nm laser (*Toptica* iBeam smart 488S-HP 200 mW) at a laser power of 100 mW. For excitation of RFP a 561 nm laser (Cobolt Jive TEM 500 mW) was used at 200 mW and 60% of output power. Images were acquired with an Andor iXon Ultra EMCCD camera driven by VisiView® Software. The gain of the camera was set to 10 and binning to 1. The exposure time differed between the transgenic lines and is indicated in the description text of each figure.

For time-lapse microscopy of the double transgenic line *Tg(mnx1:Gal4) Tg(UAS:rab7-EGFP)*, images were acquired at 37 time points with 4.9-second interval over a total duration of 3 minutes, using a 49-step z-stack with a step size of 1 µm. Similarly, imaging of the double transgenic line *Tg(mnx1:Gal4) Tg(UAS:mito-mCherry)* was performed at 16 time points with a 4.0-second interval over a total duration of 1 minute, using a 20-step z-stack with a step size of 1 µm.

3.2.1.5 Immunostaining

3.2.1.5.1 BTX Staining

Acetylcholine receptor (AChR) clusters at the neuromuscular junction (postsynapse) were labeled with α-bungarotoxin (α-BTX). Not more than ten larvae together were fixed 4% PFA PBST (1X PBS, pH 7.4, 1%DMSO, 0.1% Tween20) for 3 h at RT and subsequently washed several times in PBST (1X PBS, 0.1% Tween20). Depending on their developmental stage, larvae were permeabilized on ice with 1 mg/ml collagenase (Sigma Aldrich; #C9891) in 0.1M phosphate buffer for 45 min (2 dpf), 60 min (3 dpf), and 75 min (4 dpf). Afterwards, the larvae were incubated in pre-absorbed α-BTX Alexa Fluor™ 488 conjugate (1:100; Invitrogen/ Thermo Fisher Scientific; #B13422) in blocking solution at 4°C ON. Pre-absorbed α-BTX was obtained by incubating wild-type (wt) larvae with α-BTX at 4°C ON prior to use. The next day, the larvae were washed four times for five minutes in PBST[2] and mounted in Vectashield

mouting medium (Vector Laboratories, H-1000-10) on glass slides and stored at 4°C.

3.2.1.5.2 Acetylated/ glutamylated tubulin staining

For, visualization of F-actin in the skeletal muscle and vinculin at the myotendinous junction as well as acetylated and glutamylated tubulin, zebrafish larvae were fixed for 2h at RT in 4% PFA PBST (1X PBS, pH 7.4, 1%DMSO, 0.2% Triton X-100) and washed in PBST (1X PBS, 0.2% Triton X-100). Depending on their developmental stage, larvae were permeabilized on ice with 1 mg/ml collagenase in 0.1M phosphate buffer for 45 min (2 dpf), 60 min (3 dpf), and 75 min (4 dpf). Following permeabilization, larvae were washed again several times in PBST[1] and incubated with blocking solution (5% goat serum in PBST) for 2h at RT. For vinculin/ actin co-labelling, larvae were incubated overnight at 4°C with an anti-vinculin primary antibody (clone VIIF9 (7F9), Merck Millipore, MAB3574) at a 1:400 dilution

in blocking solution. After four washes with PBST, larvae were incubated overnight at 4°C with TRITC-conjugated phalloidin (Merck Millipore, 90228) diluted in blocking solution at 1:1000. For acetylated/ glutamylated tubulin staining, After subsequent washes in PBST, the larvae were mounted in Vectashield® mounting medium (Vector Laboratories, H-1000-10) on glass slides and stored at 4°C.

3.2.1.5.3 Activated Casp3 Immunolabeling

For, visualization of apoptosis SCs in zebrafish larvae. Zebrafish larvae at 3-days post fertilization (dpf) were fixed for 2h at RT in 4% PFA PBST (1X PBS, pH 7.4, 1%DMSO, 0.2% Triton X-100) and washed in PBST[1] (1X PBS, 0.2% Triton X-100). Larvae were permeabilized on ice with 1 mg/mL collagenase in 0.1M phosphate buffer for 60 min. Following permeabilization, larvae were washed again several times in PBST and incubated with blocking solution (5% goat serum in PBST) for 2h at RT. Next, larvae were incubated overnight

at 4°C with cleaved caspase-3 antibody (Cell Signaling, #9661T) at a 1:200 dilution in blocking solution. After four washes with PBST, larvae were incubated overnight at 4°C with anti-rabbit IgG secondary antibody Alexa Fluor™ 405 conjugate (1:400; Invitrogen/ Thermo Fisher Scientific; #A31556) in blocking solution at 4°C ON. After subsequent washes in PBST[1], the larvae were mounted in Vectashield® mounting medium (Vector Laboratories, H-1000-10) on glass slides and stored at 4°C.

3.2.1.6 Western Blot

At 4dpf, 10 siblings and 10 *cct3*-mutants were collected per tube in sample buffer (4 M Urea, 10% Glycerol, 4% SDS, 0.125 M Tris-HCl (pH 6.4), 100 mg bromphenolblue, 10 % β-mercaptoethanol) containing protease inhibitor (Sigma, P8340). Samples were denatured by heating at 60 °C for 10 minutes, followed by immediate cooling on ice. After centrifugation (13000 rpm, 5 min, 4°C), supernatants were

collected. Fifteen µl of the protein lysate was loaded per sample and separated on 4% and 10% SDS-PAGE. Proteins were transferred onto a PVDF membrane by wet blotting in transferring buffer (10%TBST, 20% MeOH). Membranes were incubated at room temperature (RT) for 15 minutes in Ponceau S. After washing with H2O, membranes were incubated for 1 hours at RT in blocking buffer (1% (w/v) Blocking Reagent (Roche, 1096176), 20mM maleic acid, 30mM NaCl, 0.8 x TBST, 0.01% thimerosal). Incubation with primary antibodies was performed over night at 4°C (TCP-1 γ antibody [1:1000; Santa Cruz; sc-271336], anti-beta actin [1:10000; Abcam, ab6276], anti-α-Tubulin [1:1000; Sigma, T5168], anti-GAPDH [1:10000, Abcam, EPR16891]). After washing in 1 x TBST membranes were incubated at RT for 2 hours with HRP-conjugated secondary antibodies (goat anti-mouse IgG [1:2000; Invitrogen; #32430], Goat anti-Rabbit IgG [1:1000; Invitrogen; #31460]). After washing in 1xTBST, band detection was

performed using the SuperSignal™ West Femto Maximum Sensitivity Substrate (Thermo Scientific™, #34095) and developed using the iBright™ FL1500 Imaging System (Invitrogen™).

3.2.1.7 Cct3 mRNA injection

First, one nl volume containing 300pg cct3 mRNA, along with 0.1 M KCl and phenol red was injected into the yolk of one-cell stage embryos using the FemtoJet 4x microinjector (Eppendorf). The concentration of cct3 mRNA was determined by injecting different concentrations into wildtype embryos. The injection needle was broken with forceps to a diameter of 0.8 mm. Thus, 3 nL of the liquid was injected into the yolk of each embryo. About half larvae of all clutches were injected, and uninjected embryos from the same clutches were used as controls. Injected versus non-injected embryos were randomly assigned to the groups. All the embryos were raised at 28°C and checked daily for malformations and the

known phenotype of cct3 homozygous mutants. Pictures of the injected anfd un injected larvae were taken on day 2/3/4 to visualize the alteration. At 5 dpf all larvae were killed, lysed with 20 µL lysis buffer and genotyped as described above to determine the homozygous mutants of injected and uninjected larvae.

3.2.2 Molecular methods

3.2.2.1 DNA Extraction from caudal fin

Fin biopsies from adult zebrafish were placed in a 0,2-mL PCR tube containing methanol. The methanol was removed, and any potential residues evaporated by incubating at 55 °C for 30 min. Then, 100 µL of lysis buffer was added. Samples were incubated at 55 °C ON. The reaction was terminated by incubating at 95 °C for 10 min which inactivated the PK. After lysis, samples were stored at -20 °C.

3.2.2.2 PCR with GoTaq® DNA Polymerase

By using PCR with Taq polymerase the gene of interest can be amplified. Zebrafish genomic

DNA was amplified from lysates of zebrafish tissue using a reaction mix containing 17,9 µl of Green Mix with 1 µl of FRW primer stock and 0.1 µl Taq polymerase. 2-4 µl of the template DNA were applied. The PCR programmes are shown in Table 14.

Table 14: Standard PCR programmes

	Step	Temperature [°C]	Duration [min/s]	Number of cycles
	Initial denaturation	94	4 min	-
PCR	Denaturation	94	30 s	39
	Annealing	52-58	30 s	
	Elongation	72	30 s	
	Final elongation	72	10 in	-

3.2.2.3 Pfu-PCR with PfuTurbo DNA Polymerase

Specific regions of genes-of-interest (GOIs) from lysates of zebrafish tissue can be amplified through Pfu-PCR. The reaction mix contained 41.5 µL of ddH_2O, 5 µL of PfuTurbo buffer, 1 µL of dNTPs (10 mM), 0.25 µL of forward and reverse primer (100 µM), 1 µL of

PfuTurbo DNA polymerase (2.5 U/µL), and 1 µL of template DNA (20 ng). Amplification was subsequently performed on a thermal cycler according to the program described as follows: 2 minutes 94°C; 35 cycles of 30 seconds 94°C, 30 seconds annealing temperature, 30 seconds 72°C and lastly 10 minutes 72°C. For both amplifications, different annealing temperatures were tested.

3.2.2.4 Restriction Enzyme Disgestion

For genotyping a digest mixture containing 12 µL of ddH_2O, 2.5 µL of 10x rCutSmart™ buffer and 0.5 µL of the respective restriction enzyme (RE) were assembled in a 0.2-mL PCR tube. To this mix, 10 µL of PCR reaction product was added. The restriction digest was performed ON and subsequently inactivated for 15 min at the temperature indicated in Table 8.

3.2.2.5 Gel electrophoresis

After PCR or digestion, the samples can be analyzed by heteroduplex mobility assay using agarose gel electrophoresis. For the genotyping, a 3% gel was used. 18 g of low melting agarose [Biozym (Hessisch Oldendorf, Germany) (#840001)] was mixed with 600 mL of TBE buffer. For the nucleic acid stain, 60 µl of Gel Red [Sigma Aldrich (St. Louis, MO, USA) (#SCT123)] was added.

3.2.2.6 Plasmid-related methods

3.2.2.6.1 TOPO TA Cloning

To sequence PCR-amplified zebrafish genomic DNA fragments, they were cloned into the pCR™2.1-TOPO™ vector using the 'TOPO™ TA Cloning™ Kit' by Invitrogen. First, amplified DNA fragments were purified from a gel and eluted in 10 µL of ddH_2O. Next, 1-2 µL or PCR product (approx. 20 ng) were mixed with 1 µL of provided salt solution and 1 µL of pCR™2.1-TOPO™ vector. The sample was brought up to a total volume of 6 µL with ddH_2O and

incubated for 30 min at 23°C. And keep the reaction on ice before proceeding with the transformation.

3.2.2.6.2 Chemical Transformation

Competent cells should be thawn on the ice. Mixing 2 µL ligated plasmid and 25 µL competent cells by stirring with the pipette tip. The mixture should be incubated on ice for 30 min. And then heat-shocked the cells for 30 seconds at 42°C and place back on ice. 125 µL for SOC medium was added at room temperature and incubated at 37 °C for 1h while shaking at 225 rpm. Finally, spreading 150 µL of the mixture on pre-warmed selective LB agar plate containing either Kanamycin (50 µg/mL) or Ampicillin (100 µg/mL) and incubated ON at 37 °C.

3.2.2.6.3 Mini preparation

A single colony of transformed TOP10 *E. coli* was inoculated into 5 mL of LB medium containing either Kanamycin (50 µg/mL) or

Ampicillin (100 µg/mL) and was incubated ON at 37°C while shaking at 225 rpm (mini culture). For harvesting, 2 mL of the culture were transferred into a 2-mL reaction tube and pelleted by centrifugation at 2000 x g for 5 min. After decanting the supernatant, 200 µL of buffer P1 with RNase were added and the pellet weas resuspended by mixing. Subsequently, 400 µL of buffer P2 and 300 µL of cold buffer P3 were added while inverting in between. Next, the sample was centrifuged at 17,900 x g (4 °C) for 10 min. The supernatant was transferred into a fresh 1.5-mL reaction tube containing 640 µL isopropanol for precipitation. This was followed, by a centrifugation step at 17,900 x g for 15 min (4 °C). Next, the pellet was washed with 70% ethanol and centrifuged at 17,900 x g for 10 min (4°C). The supernatant was removed, and the pellet was dried at RT. Finally, the pellet was resuspended in 30 µL of ddH_2O. DNA yield was validated by measuring DNA concentration using a DeNovix DS-11 FX Spectrophotometer/Fluorometer. After

measurement, the samples were stored at -20 °C until further use.

3.2.2.6.4 Midi Preparation

A single colony of transformed TOP10 *E. coli* was inoculated into 5 mL of LB medium containing either Kanamycin (50 µg/mL) or Ampicillin (100 µg/mL) and was incubated at 37°C for 8 h while shaking at 225 rpm (pre-culture). Next, 50-1000 µL of pre-culture (depending on the density) were inoculated into 50 mL of LB medium containing the respective antibiotic and was incubated ON at 37°C while shaking at 225 rpm (midi culture). After incubation, the bacteria were harvested by centrifugation at 4000 x g for 20 min (4 °C). The purification was performed using the 'NucleoBond® Xtra Midi' by Macherey-Nagel.

In brief, the harvested bacteria pellet was resuspended in 16 mL of resuspension buffer. Next, 16 mL of lysis buffer were added, and the sample was incubated for 5 min at RT. This was followed, by adding 16 mL of neutralization

buffer to terminate the lysis. In the meantime, a 'NucleoBond® Xtra Column Filter' was placed in a 'NucleoBond® Xtra Column' and equilibrated by rinsing with 12 mL of equilibration buffer. The bacterial lysate was loaded on the column filter. After the entire lysate went through the filter, a washing step with 5 mL of equilibration buffer followed. Next, the filter was discarded, and the column was washed with 8 mL of washing buffer. Subsequently, the column was eluted with 5 mL of elution buffer. For precipitation, the eluate was mixed with 3.5 mL of isopropanol, vortexed and centrifuged at 15.000 x g for 30 min (4 °C). A washing step with 2 mL of 70% ethanol followed (centrifugation at 15.000 x g for 10 min at RT). After drying, the pellet was resuspended in 200 µL of ddH_2O. The plasmid DNA concentration was measured using a DeNovix DS-11 FX Spectrophotometer/Fluorometer. Plasmid DNA was stored at -20 °C until further use.

3.2.2.7 *In vitro* RNA synthesis

3.2.2.7.1 DNA extraction from agarose gels and purification of DNA

Extraction of DNA from agarose gels was performed using the 'QIAquick Gel Extraction Kit' by Qiagen. The fragment-of-interest was cut out of the gel using a scalpel and transferred into a 2-mL-reaction tube. The gel fragment was weighed and 3 volumes of QG buffer were added to 1 gel volume. Then, the sample was incubated at RT for up to 30 min while the tube was inverted every 5-10 min. After the gel was dissolved, 1 gel volume of isopropanol was added. The mixture was applied to a QIAquick column and centrifuged at 7,900 x g for 1 min. All subsequent centrifugation steps were carried out at 7,900 x g for 1 min as well. The flow-through was discarded, 500 µL of QG buffer were applied to the column and centrifuged. Next, the column was washed with 750 µL of PE buffer. After addition of PE buffer, the column was left to stand for 5 min at RT before centrifugation. After discarding the flow-

through, another additional centrifugation step followed to remove any residual ethanol before elution. Finally, the column was eluted with 30 µL of water. After addition of water, the column was incubated for 4 min at RT before centrifugation to increase the yield of purified DNA. Additionally, the column was re-eluted with the initial elution flow-through which also gains higher DNA yield. The purified DNA was stored at -20 °C until further use.

Purification of DNA after PCRs and digests was performed using the 'QIAquick PCR Purification Kit' by Qiagen. After the PCR or digest reaction was finished, 5 volumes of PB were added to 1 volume of PCR or digest sample. The mix was applied to a QIAquick column and centrifuged at 7,900 x g for 1 min. The flow-through was discarded and 750 µL of PE buffer were applied to the column. All subsequent steps were identical to the gel extraction protocol.

3.2.2.7.2 *In vitro* RNA synthesis and purification

Synthesis of RNA for rescue microinjections was carried out using the “mMESSAGE mMACHINE™ SP6 Transcription Kit” following the manufacturer’s instructions. In brief, 1 µg of template DNA were mixed with 2µL of 10x Reaction Buffer, 10 µL of 2x NTP/CAP, 2 µL of Enzyme Mix and nuclease-free water was added to a final volume of 20 µL. The sample was gently mixed and incubated at 37 °C for 2 h. Next, 1 µL of TURBO DNase was added to the reaction, followed by an additional incubation at 37°C for 15 min. RNA was then precipitated by adding 30 µL nuclease-free water and 30 µL LiCl precipitation solution. After thorough mixing, the sample was incubated at -20°C for 30 min and then centrifuged at 4°C for 15 min at maximum speed to pellet the RNA. The supernatant was removed, and the pellet was washed once with 1 mL of 70% ethanol, followed by re-centrifugation to maximize the removal of

unincorporated nucleotides. The ethanol was then removed, and the RNA was resuspended in nuclease-free water. RNA concentration was measured using a NanoDrop spectrophotometer, and the fragment size was confirmed by RNA gel electrophoresis. Samples were stored at -80 °C until further use.

3.2.2.7.3 Agarose RNA gel electrophoresis

To verify the correct size of RNA molecules after synthesis, electrophoresis was performed using agarose gels (2% agarose dissolved in freshly prepared 0.5x TBE buffer). GelRed® was used as nucleic acid dye (1 µL per 10 mL of agarose). The duration was 1-3 h at a voltage of 80-120 V.

Before loading RNA samples on the gel, they were mixed in a 1:1 ratio with 2x RNA Loading Dye (Thermo Fisher), heated for 10 min at 70 °C and chilled on ice. RiboRuler Low Range RNA Ladder (Thermo Fisher) was prepared in the same manner before loading on the gel.

3.2.2.7.4 Sequencing

For sequencing of plasmid DNA or DNA extracted from gels, samples were sent to Microsynth AG (Göttingen, Germany). Either 1200 ng of plasmid DNA or 90 ng of PCR product were used in one reaction together with respective sequencing primers that were added at a concentration of 20 µM. For sequencing of pCR™2.1-TOPO™ the M13 forward (M13 fw, TAAAACGACGGCCAG) or reverse (M13 rev, CAGGAAACAGCTATGAC) primer was used. PCR products were sequenced by using one of the primers used for amplification.

4 Results

4.1 Characterization of cct3 loss-of-function allele

Loss-of-function alleles were created using Crispr/Cas9 and two mutant alleles were chosen for further characterization (Kamil 2023; Kraft et al., 2024). The first one is *cct3*$^{p.G54Vfs*57}$ (*cct3-1*), and the first changed amino acid is glycine at position 54 being replaced by valine. The second one is *cct3*$^{p.Gly55Serfs*57}$ (*cct3-2*), and the first changed amino acid is glycine at position 55 being replaced by serine. Both *cct3-1* and *cct3-2* have a 4 bp deletion in exon 4, which leads to a frameshift, and premature stop was detected.

4.1.1 Compound heterozygous cct3 mutation-induced phenotype

After the sgRNA injection to the zebrafish embryos, the injected embryos were raised up, and the heterozygous ones were chosen through genotyping. Compound heterozygous fish (cct3 wt/p.G54Vfs*4 heterozygous and *cct3*

wt/p.G55Sfs*3 heterozygous) were incrossed to acquire the *cct3* mutant alleles to investigate the morphological changes. The mutants die at around 5 dpf. On 3 and 4 dpf, *cct3* mutants present significantly morphological differences with *cct3* siblings. Compared to the *cct3* siblings (wild-type (wt), *cct3* wt/p.G54Vfs*4 heterozygous and *cct3* wt/p.G55Sfs*3 heterozygous), *cct3* mutants show smaller eyes, smaller size in head and body, and a slower circulation on 3 dpf (Figure 1). The difference between *cct3* siblings and *cct3* mutants become more obviously at 4 dpf. Except the size of head/body and eyes, *cct3* mutants had less black pigment along the lateral line and around the yolk sac, enlarged yolk sac and display cardiac edema (Figure 1). The trunk of *cct3* mutants also tend to be curled at 4 dpf (Figure 1).

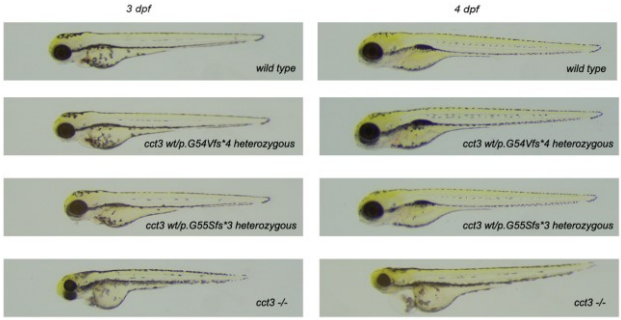

Figure 1. The morphological changes between *cct3* siblings and mutants. Images were taken at 3 and 4 dpf under the stereomicroscope. 3dpf: *cct3* mutants have smaller eyes/head, shorter body length and enlarged yolk sac. 4dpf: *cct3* mutants have smaller eyes/head, shorter body length, enlarged yolk sac, curled trunk and significantly heart edema.

4.1.2 Cct3 protein was undetectable in *cct3* mutants

To further confirm and provide additional evidence supporting the loss-of-function phenotype, Western blot was performed and cct3 protein was undetectable in mutant larvae at 4dpf (Figure 2).

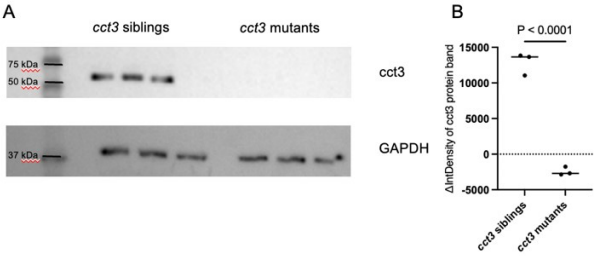

Figure 2. Western blot result of cct3 protein. The expression of cct3 is undectable in cct3 mutants, and protein levels were normalized by GAPDH expression.

4.1.3 Cct3-deficient larvae show reduced response to mechanical stimulation

In addition to morphological changes, alterations in motor function were observed. The touch-evoked response assay was performed with a metal probe. After stimulation of the anterior head region of the larvae, the touch-evoked response was obviously reduced in the *cct3* mutants compared with the *cct3* siblings (wild-type (wt), *cct3* wt/p.G54Vfs*4 heterozygous and *cct3* wt/p.G55Sfs*3 heterozygous) at 3 and 4 dpf (Figure 3).

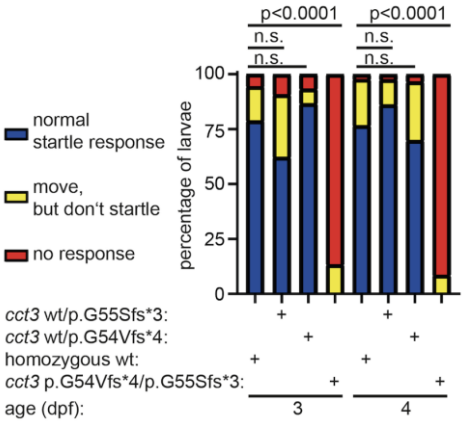

Figure 3. The touch-evoked response reduced in *cct3* mutants. Touch-evoked response assay performed under the stereomicroscope. Quantification demonstrates significantly altered touch response at 3 and 4 dpf in cct3 mutants, compared to wt and heterozygous siblings. P values were determined using Fisher's exact test.

4.1.4 Wildtype *cct3* mRNA rescues the phenotype of *cct3* mutants

To prove that the observed phenotype was specifically caused by the loss of *cct3*, cct3 mRNA microinjection was performed to assess whether the phenotype of *cct3* mutants could be rescued. After amplifying *cct3* mRNA from zebrafish cDNA and cloning it into a pCS2+ vector, the mRNA was synthesized and injected into one-cell-stage embryos as described in section 1.4.1.7. The *cct3-1*

heterozygous fish were incrossed to acquire the *cct3* mutant one-cell-stage embryos for the microinjection. About half of the larvae of two clutches were injected, and uninjected embryos from the same clutches were used as controls. The injected and uninjected larvae were collected to screen under the stereomicscope at 4 and 5 dpf. We observed a significant, but incomplete rescue of the *cct3* mutant eye and cardial edema phenotypes. Compared to the uninjected *cct3* mutants, the phenotypes were significantly reduced in mutants from the same clutches that had received 300pg of *cct3* mRNA, including smaller eyes and obvious heart edema (Figure 4).

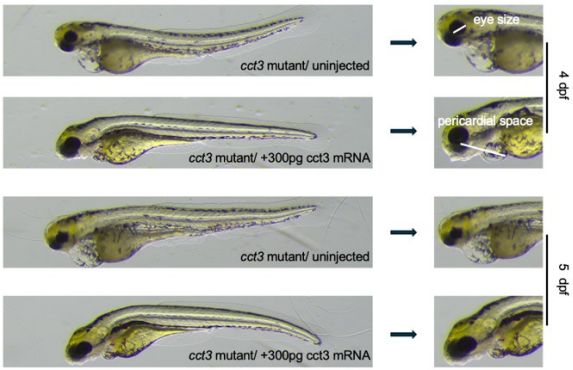

Figure 4. cct3 mRNA rescue the phenotype of *cct3* mutants. Images were aquired under the stereomicroscope at 4 and 5 dpf. The *cct3* mutants which were injected 300pg cct3 mRNA present bigger eyes and smaller pericardial space.

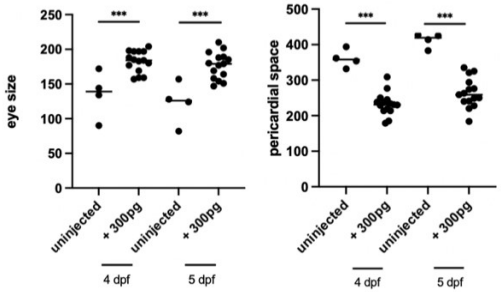

Figure 5. Quantification of the rescue experiment. Eye size of *cct3* mutants which were injected 300pg cct3 mRNA increased ($p<0.05$). Pericardial space of *cct3* mutants which were injected 300pg cct3 mRNA decreased ($p<0.05$).

4.1.5 Apoptotic Schwann cells in *cct3* mutants

Cct3 mutants display movement disorder, and patients with cct3 and other TRiC mutations also have similar clinical features and white matter issue on brain MRI (Kraft et al. 2024). So, we wanted to analyze the development of myelin sheaths. In the peripheral nervous system, myelin sheaths are formed by

Schwann cells. First, we therefore performed live imaging of the transgenic mutant line *Tg(sox10:nlsEOS) tg(Xla.Tubb:DsRed)*^{zf148} at 2, 3, and 4 dpf to determine structure of peripheral nerves as well as of associated Schwann cell nuclei.

Compared with *cct3* siblings, the number of intact Schwann cells along the peripheral nerves in *cct3* mutants was obviously decreased but the number of fragmenting Schwann cell nuclei increased at 2, 3, and 4 dpf(Figure 6). As the larvae grow older, the percentage of fragmenting Schwann cell nuclei remained unchanged. Schwann cells are neural crest derived and in the sox10 EOS line, other NC cells are labeled too. The percentage of fragmenting nuclei of NCs still at the level of the spinal cord (not migrated beyond that level) was higher in *cct3* mutants – starting from 3 dpf and more pronounced at 4 dpf.

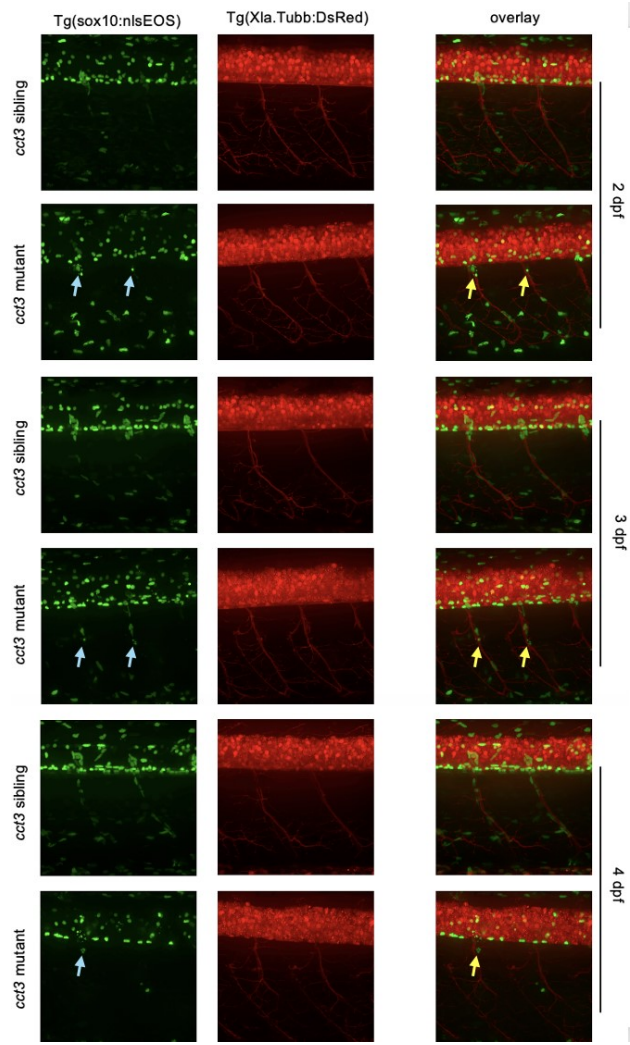

Figure 6. Live imaging of *Tg(sox10:nlsEOS) tg(Xla.Tubb:DsRed).* Neural crest-derived cells, including Schwann cells were labeled with EOS in green signals, peripheral nerves were visualized with dsRed in red signals. The apoptotic SCs fragment are shown with blue arrows(in Tg(sox10:nlsEOS)) and yellow arrows(overlay).

To determine whether fragmenting nuclei are a sign of SCs undergoing apoptosis, we performed immnolabeling of activated Caspase-3 at 3 dpf using the transgenic mutant line *Tg(sox10:nlsEOS).* Activated Caspase-3 was observed in *cct3* mutants, and the co-localization of activated caspase-3 and apoptotic SC fragmentation are also detected. In contrast, the shape of SCs in *cct3* siblings tend to be normal (Figure 7).

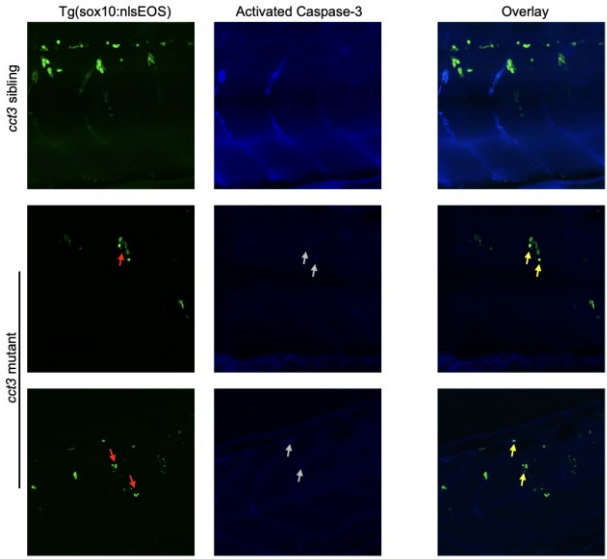

Figure 7. Results of Caspase-3 Assay. Neural crest-derived cells including Schwann cells were labeled with EOS in green signals, activated caspase-3 were excited with a 408nm laser in blue signal. Fragmental apoptotic SCs nuclei were labeled with red arrows, activated caspase-3 were labeled with grey arrows and the co-localization were labeled with yellow arrows.

4.2 *Cct3* mutants influence the function of microtubule

4.2.1 Tubulin was undetectable in cct3 mutants

Since the role of TRiC/CCT is participating in the folding of actin/tubulin, the Western Blot was performed to identify the expression of

tubulin in *cct3* siblings and mutants. Western blot analysis revealed a non-significant reduction of β-Actin, but a strong and significant reduction of β-Tubulin in *cct3* mutants compared to siblings(Figure 8).

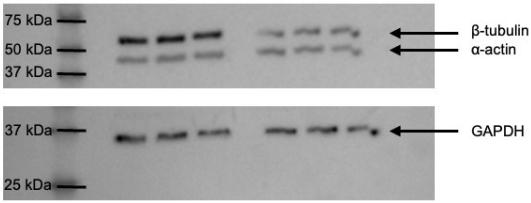

Figure 8. Western blot result of actin/tubulin. Compared to the *cct3* siblings, the expression of tubulin is reduced in *cct3* mutants, and expression of actin remains unchanged in *cct3* mutants. Protein levels were normalized by GAPDH expression.

4.2.2 Altered posttranslational modifications of tubulin were in *cct3* mutants

Since western blot shows the expression of tubulin is significantly reduced in *cct3* mutants, and posttranslational modifications of tubulin are crucial for the function of microtubules, acetylated and polyglutamylated tubulin

immunostainings were performed at 3 dpf. The distribution of acetylated tubulin in the spinal cord and along the peripheral nerves is abundant in *cct3* siblings, while in *cct3* mutants there is only very few acetylated tubulin distributed in the region close to the spinal cord (Figure 9). Glutamylated tubulin is mainly found in the distal part of the peripheral nerves (Figure 9). Compared to *cct3* siblings, the signal of glutamylated tubulin in *cct3* mutants is weaker (Figure 9).

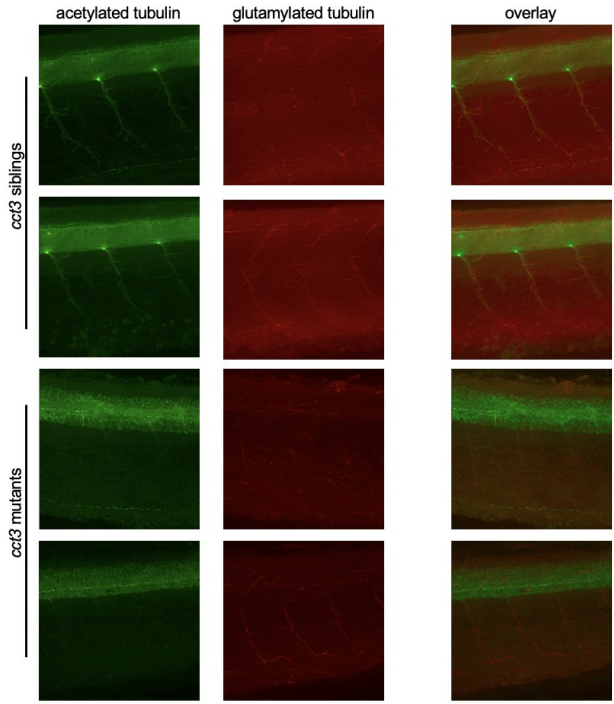

Figure 9. Results of acetylated/glutamylated tubulin immunostaining. Staining was performed using *cct3-1* fishline at 4 dpf. The acetylated tubulin was excited with a 488nm laser and labeled with green signal. The glutamylated tubulin was excited with a 561nm laser and labeled with red signals.

4.2.3 The distribution of microtubule was disrupted in *cct3* mutants

Since TRiC/CCT is known to participate in the folding of actin and tubulin, we determined the distribution of F-actin and microtubules in

peripheral nerves. The transgenic fishline *Tg(mnx1:Gal4)* was crossed with the previously established transgenic fishline *Tg(UAS:lifeact-GFP-p2a-EB3-RFP)*, and live imaging was performed using the combined fishline. The distribution of the microtubule plus-end binding protein EB3 reflects the organization of microtubules, while actin is visualized with a versatile marker - lifeact. In *cct3* siblings, the pattern of microtubules seems more organized along the axon trunk, in contrast, there're more irregular branches along the trunk in *cct3* mutants (Figure 10). Regarding F-actin, its distribution appears more uneven in *cct3* mutants compared to their siblings (Figure 10).

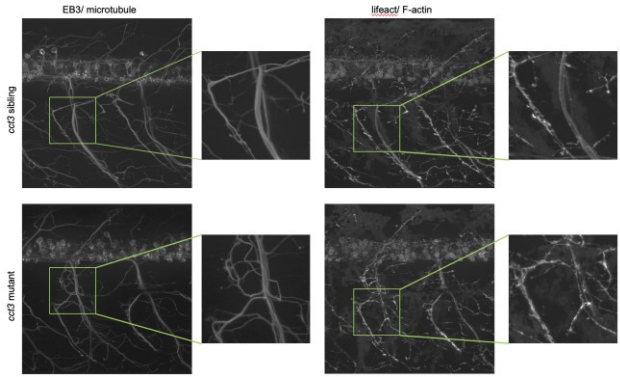

Figure 10. Distribution of F-actin and microtubules. Live imaging was performed using the transgenic fishline *Tg(mnx1:Gal4)Tg(UAS:lifeact-GFP-p2a-EB3-RFP)* at 4 dpf. The left column shows the distribution of EB3, and the right column shows the distribution of actin.

4.3 Developmental refinement of neuromuscular junction and muscle fiber architecture are disturbed in *cct3* mutants

Underdeveloped neuromuscular junctions (NMJs) were found in patients with cct3 mutation. Fluorescently labeled bungarotoxin (BTX), which binds to and labels acetylcholine receptors (AchRs) was used to visualize postsynapses of the NMJ. We performed BTX labeling in the *cct3* loss-of-function mutants at 2, 3, and 4 dpf. In *cct3* siblings, the density of

BTX-labeled synapses increases from 2 dpf to 4 dpf, while the area fraction of BTX-labeled postsynapses remained unchanged. This can be explained by a refinement of postsynapses during development, during which larger BTX-positive acetylcholine clusters decline and smaller, more refined and elaborated synaptic structures appear. In *cct3* mutants, the area fraction of BTX-labeled postsynapses didn't show significant difference compared to sibling, while the density of BTX-labeled synapses decreased a lot. This correlated with a higher percentage of larger BTX-positive acetylcholine receptor clusters (>25 μm2), indicative of deficient refining of the postsynapses over time in cct3 mutants. The quantifications are shown in Figure 13.

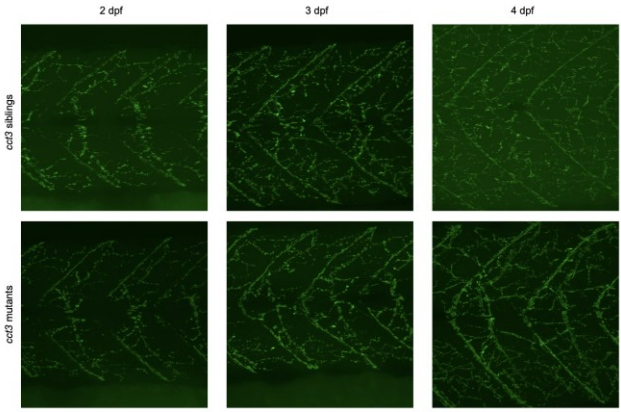

Figure 11. Results of BTX staining. Staining was performed using *cct3-1* fishline at 2, 3, and 4 dpf. The postsynaptic acetylcholine receptors (AChR) in neuromuscular junctions were labeled with the neurotoxin a-bungarotoxin (a-BTX).

Given the role of TRiC/CCT in folding of actin and tubulin, we examined F-actin distribution in skeletal muscle by phalloidin staining, combined with immunostaining for vinculin, an actin-binding protein that attaches muscle fibers at the myotendinous junction along the segment boundaries of zebrafish. In *cct3* siblings, muscle fibers were arranged in a regular and orderly pattern, while this organization was disrupted in *cct3* mutants

(Figure 12). Moreover, compared to siblings, vinculin had a tendency to be more irregular in *cct3* mutants. The quantifications are shown in Figure 13.

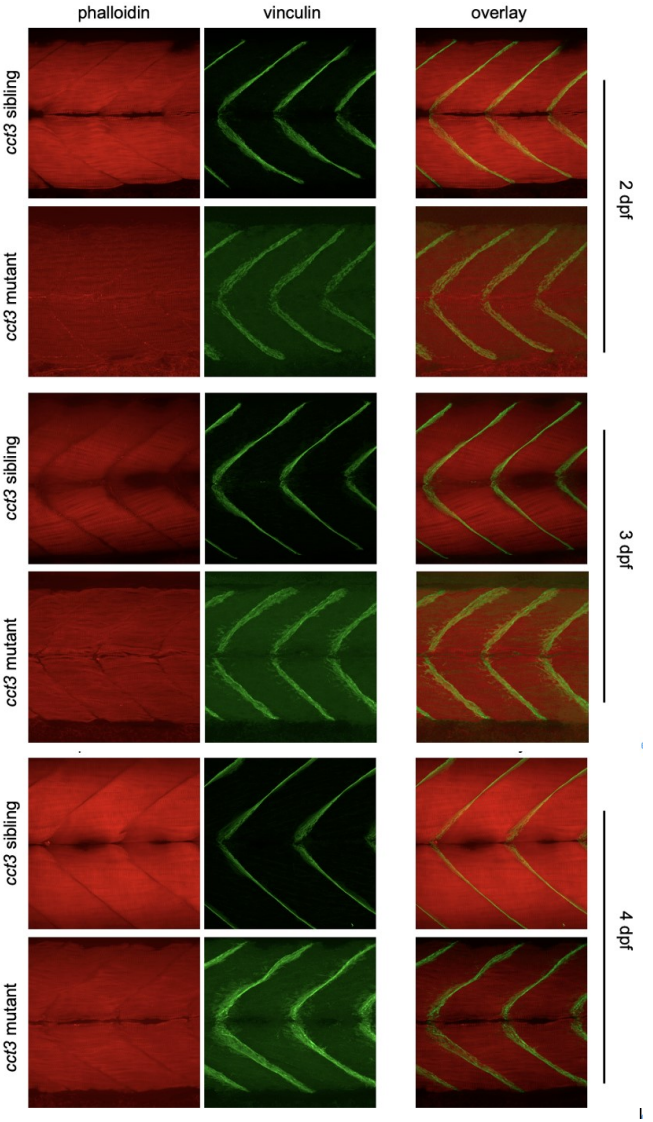

Figure 12. Results of phalloidin/vinculin staining. Staining was performed using *cct3-1* fishline at 2, 3, and 4 dpf. The F-actin were labeled with the vinculin.

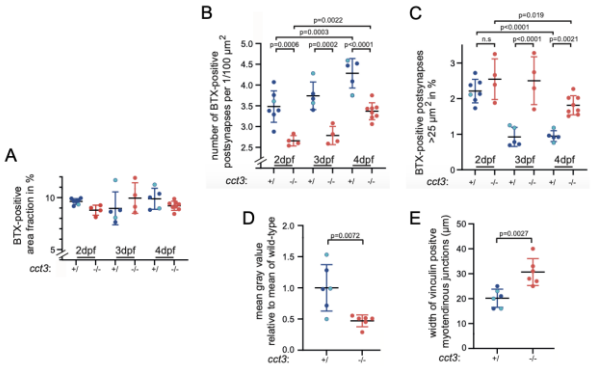

Figure 13. Quantification of BTX staining and phalloidin/vinculin staining. Quantification of the area fraction covered by BTX-positive synapses (A), density of BTX-positive postsynapses (number per area; B) and percentage of large BTX-positive postsynapses (>25 µm2) (C).Quantification of phalloidin labeling intensity (D) and width of vinculin positive myotendinous junctions (E). Heterozygous were indistinguishable from wt and therefore siblings are displayed together - wt indicated by light blue data points and heterozygous individuals by dark blue data points.

4.4 The axonal transport of organelles was disrupted in *cct3* mutants

Since *cct3* is involved in the folding of cytoskeletal proteins, including actin and tubulin, and we have observed dysfunction of tubulin in *cct3* mutants, therefore, the time lapse was performed to observe organelles axonal transport in *cct3* mutants at 2, 3, and 4

dpf. Transgenic line *Tg(UAS:mito-mCherry)* was generated to label mitochondria with mCherry, and *Tg(UAS:EGFP-Rab7)* was generated to label Rab7+ endosomes with GFP. In cct3 siblings, these organelles move fast along the nerves, while in the *cct3* mutants they tend to remain stationary or display only short back-and-forth movements (Figure 14 & Figure 15).

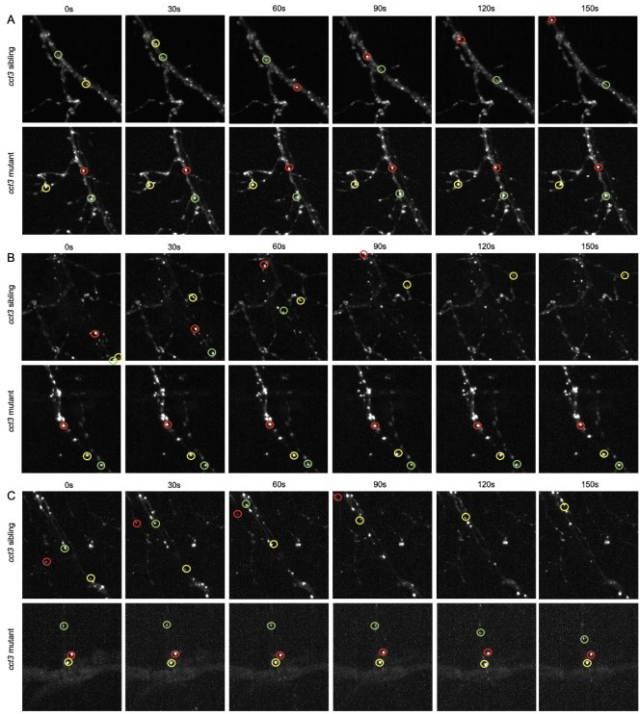

Figure 14. The time lapse images of *Tg(mnx1:Gal4)Tg(UAS:EGFP-Rab7)* at 2, 3, and 4 dpf. Individual Rab7+ endosomes were shown with same-colored circles. images were acquired at 37 time points with 4.9-second interval over a total duration of 3 minutes, using a 49-step z-stack with a step size of 1 μm.

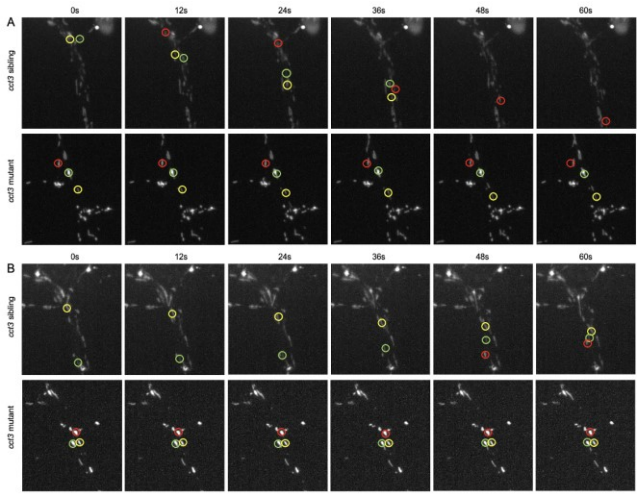

Figure 15. The time lapse images of *Tg(mnx1:Gal4) Tg(UAS:mito-mCherry)* at 3 and 4 dpf. Individual mitochondria were shown with same-colored circles. Images were acquired at 16 time points with a 4.0-second interval over a total duration of 1 minute, using a 20-step z-stack with a step size of 1 μm.

5 Discussion

TRiC/CCT is a eukaryotic chaperonin which participate in the folding of cytoskeleton proteins, including actin and tubulin, and cct3 is one of its subunits. Patients carrying *cct3* mutations exhibit movement disorder, intellectual disability, and white matter issues on brain MRI. Cct3 loss-of-function zebrafish model was generated to investigate the mechanism underlying these alterations. The *cct3* mutants display significantly morphological deficits, including decreased body size and cardiac edema, as well as behavioral abnormalities, such as the pronounced weakened touch-evoked response which appears from 2 dpf.

Loss of cct3 leads to impairment in the formation of microtubule, reflected on the altered distribution of microtubule plus-end tracking proteins (+TIPs), including EB3, disruption of acetylation and glutamylation of tubulin, and the reduced expression of tubulin shown in the western blot.

EB3, using to visualize microtubule growth events, is one of the microtubule +TIPs, a category of protein associated with the plus ends of elongating microtubules with the function of modulate their dynamics and their ability to control cell polarity (Borghi et al. 2024). PTMs of tubulin, including acetylation and glutamylation, are important for the proper function of microtubules. Axonal microtubule acetylation relies on the distribution and activity of α-tubulin acetyltransferase (ATAT1) (Even et al. 2019), while histone deacetylases (HDACs) enhance the microtubule deacetylation (Li et al. 2011). Acetylated tubulin combines with the motor proteins, including kinesin and dynein, whereas deacetylation decreases the speed of axonemal kinesin/dynein, which also reflected in the impaired axonal transport of Rab7+ endosomes and mitochondria in the cct3 loss-of-function variant (Nekooki-Machida & Hagiwara 2020). Abnormal tubulin acetylation is widely reported in neurodegenerative disorders. In Alzheimer's disease, MAP Tau

preferentially binds to acetylated tubulin and stabilizes microtubules. In Huntington's disease, HDACs inhibition improves axonal transport deficits by enhancing tubulin acetylation (Dompierre et al. 2007). These findings also provide new potential therapeutic targets for neurodegenerative disorders. Cytosolic carboxy peptidases (CCPs), which function as deglutamylase enzymes, play a crucial role in maintaining proper glutamylation status of microtubules (Sheikh & Tabassum 2024). A study found that patients with progressive neurodegenerative disease with onset in infancy carry loss-of-function mutations in the CCP1 gene and dysregulation of tubulin polyglutamylation was detected in mice with inactivating variants in the gene for CCP1 (Rogowski et al. 2019; Shashi et al. 2018). Microtubule glutamylation enhances the binding affinity of both kinesin and dynein (Sheikh & Tabassum 2024) and reduced glutamylated tubulin leads to abnormalities in axonal transport. Glutamylase TTLL1

polyglutamylates α-tubulin, and loss of TTLL1 leads to increased mitochondria motility in neurons of the mouse model (Bodakuntla et al. 2021), which was also found in the cct3 loss-of-function variant.

Muscle biopsy from the patient carrying *cct3* mutation present underdeveloped neuromuscular junctions (NMJs) (Kraft et al. 2024), a phenotype that was similarly found in the *cct3* loss-of-function zebrafish model. The formation and maintenance of the NMJ depend on the Agrin/ Lrp4/ MuSK signaling pathway (Sun et al. 2024). Agrin is a protein secreted by motor neurons and released into the synaptic cleft during the development of the NMJ. Agrin/ Lrp4/ MuSK pathway promotes the clustering of acetylcholine receptors (AChRs) at the postsynaptic membrane and ensures efficient neurotransmission at the NMJ. Zebrafish lacking agrin show movement impairments(Sun et al. 2024). NT1654, a synthetic agrin fragment, has been shown to rescue the MYO9A knockout mice which is an established model

related to the Congenital Myasthenic Syndromes (CMS) and exhibit the phenotype of reduced AchRs (O'Connor et al. 2019). And it also provides promising therapeutic targets for neuromuscular disorders.

In addition to the specific phenotype, apoptotic sox10+ neural crest derived cells, including Schwann cells, were also observed from 2 dpf, indicating that the dysfunction of SCs involved in the underlying mechanism. Axonal transport, which includes organelles such as endosomes and mitochondria, is disrupted in *cct3* loss-of-function variant, indicating an essential role for cct3 in maintaining proper axonal transport. Dysfunction of acetylated tubulin also contributes to the disruption. Organelles, protein complexes and mRNAs move quickly along axons, often maintaining persistent directionality over long distances. Defects in the microtubule-based machinery can cause or contribute to various neurodegenerative diseases (Saxton & Hollenbeck 2012). In Huntington's disease, expression of mutant

huntingtin (mHTT) impairs brain-derived neurotrophic factor (BDNF) transport in BACHD cortical axons (Zhao et al. 2016). Both CCT3 and the apical domains of CCT1 (ApiCCT1) can restore impaired anterograde BDNF transport and normalize retrograde BDNF transport (Zhao et al. 2016). Notably, treatment of BACHD cortical neurons with ApiCCT1 prevents striatal neuronal atrophy by enhancing BDNF release, which subsequently signals through the TrkB receptor on striatal neurons (Zhao et al. 2016). Moreover, supplementation of muscles with BDNF, but not other neurotrophins, also fully restores physiological axonal transport in Charcot-Marie-Tooth disease (CMT) mouse model (Sleigh et al. 2023).

In summary, as a main component of TRiC/CCT, CCT3 plays an essential role in the folding of cytoskeletal proteins and influence the microtubule formation and axonal transport.

6 Summary

Background: Mutations in *CCT* genes, including *CCT3* cause neurodevelopmental disorders in humans associated with cerebellar hypoplasia and reduced myelination. These roles of *cct3* in neurodevelopment are conserved in zebrafish. CCT3 is an essential subunit of TRiC/CCT, a chaperonin responsible for folding of ~10% of the proteome, including actin and tubulin.

Aims: In this thesis, I aimed at further characterizing the phenotype of *cct3* mutant larvae. More precisely, I aimed at (1) demonstrating that the observed phenotypes were due to loss of Cct3 function and furthermore, I characterized the following aspect: (2) motor behavioral response following mechanical stimulation, (3) development of the neuromuscular junctions, (4) number and survival of Schwann cells - the myelinating glial cells in the peripheral nervous system – as well as (5) axonal cytoskeleton and axonal transport.

Methods: To reach these aims, I applied several molecular methods, including Western blots, stainings and immunolabelings. Furthermore, I combined the *cct3* mutant allele with different transgenic lines that fluorescently label cells and subcellular organelles in neurons and performed live imaging on a spinning disc confocal microscope.

Results: Compound heterozygous larvae were indistinguishable from homozygous mutants and furthermore, wildtype *cct3* mRNA microinjections partially rescued the mutant phenotype, confirming that the observed mutant phenotypes were due to the loss of Cct3. I found that zebrafish *cct3* mutant larvae responded significantly less to mechanical stimulation and had an impaired developmental refinement of neuromuscular junctions. I demonstrated that Schwann cells were particularly sensitive to loss of Cct3 and underwent apoptotic cell death as early as 2 days of development, when surrounding cells were still intact. Furthermore, I observed an

altered axonal cytoskeleton as well as an impaired axonal transport of organelles.

Conclusion: As a main component of TRiC/CCT, Cct3 plays an essential role in neurodevelopment by being required for synaptic refinement, microtubule biology, axonal transport as well as Schwann cell survival.

Zusammenfassung

Hintergrund: Mutationen in *CCT*-Genen verursachen beim Menschen Neuroentwicklungsstörungen mit Kleinhirnhypoplasie und reduzierter Myelinisierung. Das Chaperonin TRiC/CCT besteht aus acht Untereinheiten und ist wichtig die Faltung von ~10 % des Proteoms, u.a. von Aktin und Tubulin. Die Funktion von Cct3 in der Neuroentwicklung ist im Zebrafisch konserviert.
Zielsetzung: Ziel dieser Arbeit war die weitere Charakterisierung des Phänotyps von Larven mit homozygoter *loss-of-function cct3*-Mutation. Konkret beabsichtigte ich zu zeigen, (1) dass die beobachteten Phänotypen auf einen Funktionsverlust von Cct3 zurückzuführen sind sowie folgende Aspekte zu untersuchen: (2) die motorische Verhaltensantwort auf mechanische Stimulation, (3) die Entwicklung der neuromuskulären Synapsen, (4) Anzahl und Überleben der Schwann-Zellen – der myelinisierenden Gliazellen des peripheren

Nervensystems und (5) das axonale Zytoskelett und den axonalen Transport.

Methoden: Ich habe verschiedene molekularbiologische Methoden, einschließlich Western Blots, Färbungen und Immunmarkierungen angewandt. Außerdem habe ich das *cct3-loss-of-function* Allel mit unterschiedlichen transgenen Linien kombiniert, um Zellen und subzelluläre Organellen in Neuronen mit fluoreszierenden Proteinen zu markieren und die resultierenden Linien am Spinning-Disk-Konfokalmikroskop zu untersuchen.

Ergebnisse: Compound-heterozygote Larven waren von homozygoten Mutanten nicht zu unterscheiden. Zudem reduzierte die Mikroinjektion von wildtypischer *cct3*-mRNA in *cct3* Mutanten deren Phänotyp, was bestätigte, dass der beobachtete Phänotyp auf den Verlust von Cct3 zurückzuführen ist. Zebrafisch *cct3*-Mutanten reagierten signifikant weniger auf mechanische Stimulation und zeigten eine reduzierte entwicklungsabhängige Reifung der

neuromuskulären Synapsen. Des Weiteren erwiesen sich Schwann-Zellen als besonders empfindlich gegenüber dem Verlust von Cct3, sie zeigten bereits ab dem zweiten Entwicklungstag apoptotischen Zelltod, während umliegende Zellen noch intakt waren. Ich konnte außerdem Veränderungen des axonalen Zytoskeletts sowie des axonalen Transports von Organellen nachweisen.

Schlussfolgerung: Als essenzielle Untereinheit des TRiC/CCT-Komplexes spielt Cct3 eine zentrale Rolle in der Neuroentwicklung, da es für die synaptische Reifung, die Mikrotubuli-Biologie, den axonalen Transport sowie das Überleben von Schwann-Zellen erforderlich ist.

7 References

Akhmanova A., Hoogenraad C.C.: Microtubule Minus-End-Targeting Proteins. Current Biology. (2015) 25: 162–171

Al-Bassam J., Kim H., Brouhard G., van Oijen A., Harrison S.C., Chang F.: CLASP Promotes Microtubule Rescue by Recruiting Tubulin Dimers to the Microtubule. Developmental Cell. (2010) 19: 245–258

Alves-Silva J., Sanchez-Soriano N., Beaven R., Klein M., Parkin J., Millard T.H., Bellen H.J., Venken K.J.T., Ballestrem C., Kammerer R.A., Prokop A.: Spectraplakins Promote Microtubule-Mediated Axonal Growth by Functioning As Structural Microtubule-Associated Proteins and EB1-Dependent +TIPs (Tip Interacting Proteins). Journal of Neuroscience. (2012) 32: 9143–9158

Arancibia-Carcamo I.L., Attwell D.: The node of Ranvier in CNS pathology. Acta Neuropathol. (2014) 128: 161–175

Arens J., Duong T.-T., Dehmelt L.: A morphometric screen identifies specific roles for microtubule-regulating genes in neuronal development of P19 stem cells. PLoS ONE. (2013) 8: 1-10

Avila J.: Microtubule functions. Life Sciences. (1992) 50: 327–334

Baron W., Hoekstra D.: On the biogenesis of myelin membranes: sorting, trafficking and cell polarity. FEBS Letters. (2010) 584: 1760–1770

Bauer N.G., Richter-Landsberg C., Ffrench-Constant C.: Role of the oligodendroglial cytoskeleton in differentiation and myelination. Glia. (2009) 57: 1691–1705

Baumann N., Pham-Dinh D.: Biology of Oligodendrocyte and Myelin in the Mammalian Central Nervous System. Physiological Reviews. (2001) 81: 871–927

Ben-Maimon M., Elad N., Naveh-Tassa S., Levy Y., Horovitz A.: Inhibition of tau

aggregation by the CCT3 and CCT7 apical domains. Protein Science. (2025) 34: 1-10

Bodakuntla S., Yuan X., Genova M., Gadadhar S., Leboucher S., Birling M., Klein D., Martini R., Janke C., Magiera M.M., Bodakuntla S., Yuan X., Genova M., Gadadhar S., Leboucher S., Birling M., Klein D., Martini R., Janke C., Magiera M.M., Bodakuntla S., Yuan X., Genova M., Gadadhar S., Leboucher S., Birling M., Klein D., Martini R., Janke C., Magiera M.M.: Distinct roles of α- and β-tubulin polyglutamylation in controlling axonal transport and in neurodegeneration. The EMBO Journal. (2021) 40: 1-15

Borghi R., Petrini S., Apollonio V., Trivisano M., Specchio N., Moreno S., Bertini E., Tartaglia M., Compagnucci C.: Altered cytoskeleton dynamics in patient-derived iPSC-based model of PCDH19

clustering epilepsy. Front Cell Dev Biol. (2024) 12: 1-13

Bouhouche A., Benomar A., Bouslam N., Chkili T., Yahyaoui M.: Mutation in the epsilon subunit of the cytosolic chaperonin-containing t-complex peptide-1 (Cct5) gene causes autosomal recessive mutilating sensory neuropathy with spastic paraplegia. J Med Genet.(2006) 43: 441–443

Bowne-Anderson H., Hibbel A., Howard J.: Regulation of Microtubule Growth and Catastrophe: Unifying Theory and Experiment. Trends in Cell Biology. (2015) 25: 769–779

Bowne-Anderson H., Zanic M., Kauer M., Howard J.: Microtubule dynamic instability: A new model with coupled GTP hydrolysis and multistep catastrophe. BioEssays. (2013) 35: 452–461

Cario A., Berger C.L.: Tau, microtubule dynamics, and axonal transport: New

paradigms for neurodegenerative disease. BioEssays. (2023) 45: 1-21

Castelnovo L.F., Caffino L., Bonalume V., Fumagalli F., Thomas P., Magnaghi V.: Membrane Progesterone Receptors (mPRs/PAQRs) Differently Regulate Migration, Proliferation, and Differentiation in Rat Schwann Cells. J Mol Neurosci. (2020) 70: 433–448

Chaaban S., Brouhard G.J.: A microtubule bestiary: structural diversity in tubulin polymers. MBoC. (2017) 28: 2924–2931

Colello R.J., Pott U.: Signals that initiate myelination in the developing mammalian nervous system. Mol Neurobiol. (1997) 15: 83–100

de Castro F., Bribián A.: The molecular orchestra of the migration of oligodendrocyte precursors during development. Brain Research Reviews. (2005) 49: 227–241

Dehmelt L., Halpain S.: The MAP2/Tau family of microtubule-associated proteins. Genome Biol. (2005) 6: 204

Desai A., Mitchison T.J.: MICROTUBULE POLYMERIZATION DYNAMICS. Annu. Rev Cell Dev Biol. (1997) 13: 83–117

Dimou L., Simon C., Kirchhoff F., Takebayashi H., Götz M.: Progeny of Olig2-expressing progenitors in the gray and white matter of the adult mouse cerebral cortex. J Neurosci. (2008) 28: 10434–10442

Dompierre J.P., Godin J.D., Charrin B.C., Cordelières F.P., King S.J., Humbert S., Saudou F., Dompierre J.P., Godin J.D., Charrin B.C., Cordelières F.P., King S.J., Humbert S., Saudou F., Dompierre J.P., Godin J.D., Charrin B.C., Cordelières F.P., King S.J., Humbert S., Saudou F.: Histone Deacetylase 6 Inhibition Compensates for the Transport Deficit in Huntington's Disease by Increasing Tubulin

Acetylation. J Neurosci. (2007) 27: 3571–3583

Dutta R., Chang A., Doud M.K., Kidd G.J., Ribaudo M.V., Young E.A., Fox R.J., Staugaitis S.M., Trapp B.D.: Demyelination causes synaptic alterations in hippocampi from multiple sclerosis patients. Annals of Neurology. (2011) 69: 445–454

Edgar J.M., McLaughlin M., Yool D., Zhang S.-C., Fowler J.H., Montague P., Barrie J.A., McCulloch M.C., Duncan I.D., Garbern J., Nave K.A., Griffiths I.R.: Oligodendroglial modulation of fast axonal transport in a mouse model of hereditary spastic paraplegia. J Cell Biol. (2004) 166: 121–131

Even A., Morelli G., Broix L., Scaramuzzino C., Turchetto S., Gladwyn-Ng I., Le Bail R., Shilian M., Freeman S., Magiera M.M., Jijumon A.S., Krusy N., Malgrange B., Brone B., Dietrich P., Dragatsis I., Janke C., Saudou F., Weil M., Nguyen

L., Even A., Morelli G., Broix L., Scaramuzzino C., Turchetto S., Gladwyn-Ng I., Le Bail R., Shilian M., Freeman S., Magiera M.M., Jijumon A.S., Krusy N., Malgrange B., Brone B., Dietrich P., Dragatsis I., Janke C., Saudou F., Weil M., Nguyen L., Even A., Morelli G., Broix L., Scaramuzzino C., Turchetto S., Gladwyn-Ng I., Le Bail R., Shilian M., Freeman S., Magiera M.M., Jijumon A.S., Krusy N., Malgrange B., Brone B., Dietrich P., Dragatsis I., Janke C., Saudou F., Weil M., Nguyen L.: ATAT1-enriched vesicles promote microtubule acetylation via axonal transport. Sci Adv. (2019) 5: 1-15

Fünfschilling U., Supplie L.M., Mahad D., Boretius S., Saab A.S., Edgar J., Brinkmann B.G., Kassmann C.M., Tzvetanova I.D., Möbius W., Diaz F., Meijer D., Suter U., Hamprecht B., Sereda M.W., Moraes C.T., Frahm J.,

Goebbels S., Nave K.-A.: Glycolytic oligodendrocytes maintain myelin and long-term axonal integrity. Nature. (2012) 485: 517–521

Geraldo S., Khanzada U.K., Parsons M., Chilton J.K., Gordon-Weeks P.R.: Targeting of the F-actin-binding protein drebrin by the microtubule plus-tip protein EB3 is required for neuritogenesis. Nat Cell Biol. (2008) 10: 1181–1189

Gestaut D., Limatola A., Joachimiak L., Frydman J.: The ATP-powered gymnastics of TRiC/CCT: an asymmetric protein folding machine with a symmetric origin story. Current Opinion in Structural Biology. (2019) 55: 50–58

Gestaut D., Zhao Y., Park J., Ma B., Leitner A., Collier M., Pintilie G., Roh S.-H., Chiu W., Frydman J.: Structural visualization of the tubulin folding

pathway directed by human chaperonin TRiC/CCT. Cell. (2022) 185: 4770-4787

Goodson H.V., Jonasson E.M.: Microtubules and Microtubule-Associated Proteins. Cold Spring Harb Perspect Biol. (2018) 10:1-20

Grantham J.: The Molecular Chaperone CCT/TRiC: An Essential Component of Proteostasis and a Potential Modulator of Protein Aggregation. Front Genet. (2020) 11: 172

Hill R.A., Li A.M., Grutzendler J.: Lifelong cortical myelin plasticity and age-related degeneration in the live mammalian brain. Nat Neurosci. (2018) 21: 683–695

Hinckelmann M.-V., Zala D., Saudou F.: Releasing the brake: restoring fast axonal transport in neurodegenerative disorders. Trends in Cell Biology. (2013) 23: 634–643

Hipp M.S., Park S.-H., Hartl F.U.: Proteostasis impairment in protein-misfolding and -

aggregation diseases. Trends in Cell Biology. (2014) 24: 506–514

Hirokawa N., Noda Y., Tanaka Y., Niwa S.: Kinesin superfamily motor proteins and intracellular transport. Nat Rev Mol Cell Biol. (2009) 10: 682–696

Horovitz A., Reingewertz T.H., Cuéllar J., Valpuesta J.M.: Chaperonin Mechanisms: Multiple and (Mis)Understood. Annu Rev Biophys. (2022) 51: 115–133

Howard J., Hyman A.A.: Microtubule polymerases and depolymerases. Current Opinion in Cell Biology. (2007) 19: 31–35

Hughes E.G., Kang S.H., Fukaya M., Bergles D.E.: Oligodendrocyte progenitors balance growth with self-repulsion to achieve homeostasis in the adult brain. Nat Neurosci. (2013) 16: 668–676

Hughes E.G., Orthmann-Murphy J.L., Langseth A.J., Bergles D.E.: Myelin remodeling through experience-

dependent oligodendrogenesis in the adult somatosensory cortex. Nat Neurosci. (2018) 21: 696–706

Jaworski J., Kapitein L.C., Gouveia S.M., Dortland B.R., Wulf P.S., Grigoriev I., Camera P., Spangler S.A., Di Stefano P., Demmers J., Krugers H., Defilippi P., Akhmanova A., Hoogenraad C.C.: Dynamic Microtubules Regulate Dendritic Spine Morphology and Synaptic Plasticity. Neuron. (2009) 61: 85–100

Jiménez-Mateos E.M., Paglini G., González-Billault C., Cáceres A., Avila J.: End binding protein-1 (EB1) complements microtubule-associated protein-1B during axonogenesis. J of Neuroscience Research. (2005) 80: 350–359

Jin M., Liu C., Han W., Cong Y.: TRiC/CCT Chaperonin: Structure and Function. Subcell Biochem. (2019) 93: 625–654

Kang M., Yao Y.: Laminin regulates oligodendrocyte development and myelination. Glia. (2022) 70: 414–429

Kassmann C.M., Nave K.-A.: Oligodendroglial impact on axonal function and survival – a hypothesis. Curr Opin Neurol. (2008) 21: 235–241

Kidd G.J., Ohno N., Trapp B.D.: Biology of Schwann cells. Handb Clin Neurol. (2013) 115: 55–79

Kinoshita K., Arnal I., Desai A., Drechsel D.N., Hyman A.A.: Reconstitution of physiological microtubule dynamics using purified components. Science. (2001) 294: 1340–1343

Klena N., Pigino G.: Structural Biology of Cilia and Intraflagellar Transport. Annu Rev Cell Dev Biol. (2022) 38: 103–123

Komarova Y., De Groot C.O., Grigoriev I., Gouveia S.M., Munteanu E.L., Schober J.M., Honnappa S., Buey R.M., Hoogenraad C.C., Dogterom M., Borisy G.G., Steinmetz M.O., Akhmanova A.:

Mammalian end binding proteins control persistent microtubule growth. J Cell Biol. (2009) 184: 691–706

Kraft F., Rodriguez-Aliaga P., Yuan W., Franken L., Zajt K., Hasan D., Lee T.-T., Flex E., Hentschel A., Innes A.M., Zheng B., Julia Suh D.S., Knopp C., Lausberg E., Krause J., Zhang X., Trapane P., Carroll R., McClatchey M., Fry A.E., Wang L., Giesselmann S., Hoang H., Baldridge D., Silverman G.A., Radio F.C., Bertini E., Ciolfi A., Blood K.A., de Sainte Agathe J.-M., Charles P., Bergant G., Čuturilo G., Peterlin B., Diderich K., Streff H., Robak L., Oegema R., van Binsbergen E., Herriges J., Saunders C.J., Maier A., Wolking S., Weber Y., Lochmüller H., Meyer S., Aleman A., Polavarapu K., Nicolas G., Goldenberg A., Guyant L., Pope K., Hehmeyer K.N., Monaghan K.G., Quade A., Smol T., Caumes R., Duerinckx S., Depondt C., Van

Paesschen W., Rieubland C., Poloni C., Guipponi M., Arcioni S., Meuwissen M., Jansen A.C., Rosenblum J., Haack T.B., Bertrand M., Gerstner L., Magg J., Riess O., Schulz J.B., Wagner N., Wiesmann M., Weis J., Eggermann T., Begemann M., Roos A., Häusler M., Schedl T., Tartaglia M., Bremer J., Pak S.C., Frydman J., Elbracht M., Kurth I.: Brain malformations and seizures by impaired chaperonin function of TRiC. Science. (2024) 386: 516–525

Lappe-Siefke C., Goebbels S., Gravel M., Nicksch E., Lee J., Braun P.E., Griffiths I.R., Nave K.-A.: Disruption of Cnp1 uncouples oligodendroglial functions in axonal support and myelination. Nat Genet. (2003) 33: 366–374

Li G., Jiang H., Chang M., Xie H., Hu L., Li G., Jiang H., Chang M., Xie H., Hu L., Li G., Jiang H., Chang M., Xie H., Hu L.: HDAC6 α-tubulin deacetylase: A potential therapeutic target in

neurodegenerative diseases. Journal of the Neurological Sciences. (2011) 304: 1–8

Ligon L.A., LaMonte B.H., Wallace K.E., Weber N., Kalb R.G., Holzbaur E.L.F., Ligon L.A., LaMonte B.H., Wallace K.E., Weber N., Kalb R.G., Holzbaur E.L.F.: Mutant superoxide dismutase disrupts cytoplasmic dynein in motor neurons. NeuroReport. (2005) 16: 533–536

Llorens F., Gil V., del Río J.A.: Emerging functions of myelin-associated proteins during development, neuronal plasticity, and neurodegeneration. The FASEB Journal. (2011) 25: 463–475

Logan C.M., Menko A.S.: Microtubules: Evolving roles and critical cellular interactions. Exp Biol Med. (2019) 244: 1240–1254

Ma X., Lu C., Chen Y., Li S., Ma N., Tao X., Li Y., Wang J., Zhou M., Yan Y.-B., Li P., Heydari K., Deng H., Zhang M., Yi C., Ge L.: CCT2 is an aggrephagy receptor

for clearance of solid protein aggregates. Cell. (2022) 185: 1325-1345

Meng X., Maurel P., Lam I., Heffernan C., Stiffler M.A., McBeath G., Salzer J.L.: Necl-4/Cadm4 recruits Par-3 to the Schwann cell adaxonal membrane. Glia. (2019) 67: 884–895

Millecamps S., Julien J.-P.: Axonal transport deficits and neurodegenerative diseases. Nat Rev Neurosci. (2013) 14: 161–176

Min W., Angileri F., Lu, H., Lauria A., Shanmugasundaram M., Almerico A.M., Cappello F., de Macario E.C., Lednev I.K., Macario A.J.L., Robb F.T.: A human CCT5 gene mutation causing distal neuropathy impairs hexadecamer assembly in an archaeal model. Sci Rep. (2014) 4: 1-9

Mitchison T., Kirschner M.: Dynamic instability of microtubule growth. Nature. (1984) 312: 237–242

Monk K.R., Feltri M.L., Taveggia C.: New insights on Schwann cell development. Glia. (2015) 63: 1376–1393

Morrison E.E., Moncur P.M., Askham J.M.: EB1 identifies sites of microtubule polymerisation during neurite development. Molecular Brain Research. (2002) 98: 145–152

Narine M., Colognato H.: Current Insights Into Oligodendrocyte Metabolism and Its Power to Sculpt the Myelin Landscape. Front Cell Neurosci. (2022) 16:1-17

Nave K.-A.: Myelination and support of axonal integrity by glia. Nature. (2010) 468: 244–252

Nave K.-A., Werner H.B.: Myelination of the Nervous System: Mechanisms and Functions. Annu Rev Cell Dev Biol. (2014) 30: 503–533

Nekooki-Machida Y., Hagiwara H.: Role of tubulin acetylation in cellular functions and diseases. Med Mol Morphol. (2020) 53: 191–197

Niwa S., Takahashi H., Hirokawa N.: β-Tubulin mutations that cause severe neuropathies disrupt axonal transport. EMBO J. (2013) 32: 1352–1364

Nogales E.: Structural Insights into Microtubule Function. Annu Rev Biochem. (2000) 69: 277–302

Noormohammadi A., Khodakarami A., Gutierrez-Garcia R., Lee H.J., Koyuncu S., König T., Schindler C., Saez I., Fatima A., Dieterich C., Vilchez D.: Somatic increase of CCT8 mimics proteostasis of human pluripotent stem cells and extends C. elegans lifespan. Nat Commun. (2016) 7: 1-15

O'Connor E., Cairns G., Spendiff S., Burns D., Hettwer S., Mäder A., Müller J., Horvath R., Slater C., Roos A., Lochmüller H.: Modulation of Agrin and RhoA Pathways Ameliorates Movement Defects and Synapse Morphology in MYO9A-Depleted Zebrafish. Cells. (2019) 8: 1-20

Ommer A., Figlia G., Pereira J.A., Datwyler A.L., Gerber J., DeGeer J., Lalli G., Suter U.: Ral GTPases in Schwann cells promote radial axonal sorting in the peripheral nervous system. J Cell Biol. (2019) 218: 2350–2369

Pavel M., Imarisio S., Menzies F.M., Jimenez-Sanchez M., Siddiqi F.H., Wu X., Renna M., O'Kane C.J., Crowther D.C., Rubinsztein D.C.: CCT complex restricts neuropathogenic protein aggregation via autophagy. Nat Commun. (2016) 7: 1-18

Perlson E., Jeong G.-B., Ross J.L., Dixit R., Wallace K.E., Kalb R.G., Holzbaur E.L.F., Perlson E., Jeong G.-B., Ross J.L., Dixit R., Wallace K.E., Kalb R.G., Holzbaur E.L.F.: A Switch in Retrograde Signaling from Survival to Stress in Rapid-Onset Neurodegeneration. J. Neurosci. (2009) 29: 9903–9917

Perlson E., Maday S., Fu M., Moughamian A.J., Holzbaur E.L.F., Perlson E.,

Maday S., Fu M., Moughamian A.J., Holzbaur E.L.F.: Retrograde axonal transport: pathways to cell death. Trends in Neurosciences. (2010) 33: 335–344

Podbielska M., Hogan E.: Molecular and immunogenic features of myelin lipids: incitants or modulators of multiple sclerosis. Mult Scler. (2009) 15: 1011–1029

Pollard T.D., Goldman R.D.: Overview of the Cytoskeleton from an Evolutionary Perspective. Cold Spring Harb Perspect Biol. (2018) 10: 1-7

Rogowski K., van der Laan S., Dubra G.: Tubulin glutamylation: a skeleton key for neurodegenerative diseases. Neural Regen Res. (2019) 14: 1899-1900

Rowitch D.H.: Glial specification in the vertebrate neural tube. Nat Rev Neurosci. (2004) 5: 409–419

Sabry J., O'Connor T.P., Kirschner M.W.: Axonal transport of tubulin in Ti1

pioneer neurons in situ. Neuron. (1995) 14: 1247–1256

Salzer J.L.: Schwann cell myelination. Cold Spring Harb Perspect Biol. (2015) 7: 1-26

Saxton W.M., Hollenbeck P.J.: The axonal transport of mitochondria. J Cell Sci. (2012) 125: 2095–2104

Shashi V., Magiera M.M., Klein D., Zaki M., Schoch K., Rudnik-Schöneborn S., Norman A., Lopes Abath Neto O., Dusl M., Yuan X., Bartesaghi L., De Marco P., Alfares A.A., Marom R., Arold S.T., Guzmán-Vega F.J., Pena L.D., Smith E.C., Steinlin M., Babiker M.O., Mohassel P., Foley A.R., Donkervoort S., Kaur R., Ghosh P.S., Stanley V., Musaev D., Nava C., Mignot C., Keren B., Scala M., Tassano E., Picco P., Doneda P., Fiorillo C., Issa M.Y., Alassiri A., Alahmad A., Gerard A., Liu P., Yang Y., Ertl-Wagner B., Kranz P.G., Wentzensen I.M., Stucka R.,

Stong N., Allen A.S., Goldstein D.B., Schoser B., Rösler K.M., Alfadhel M., Capra V., Chrast R., Strom T.M., Kamsteeg E., Bönnemann C.G., Gleeson J.G., Martini R., Janke C., Senderek J.: Loss of tubulin deglutamylase CCP1 causes infantile-onset neurodegeneration. The EMBO Journal. (2018) 37: 1-12

Sheikh A.Md., Tabassum S.: Potential role of tubulin glutamylation in neurodegenerative diseases. Neural Regen Res. (2024) 19: 1191–1192

Shu L., Huang X., Cheng X., Li X.: Emerging Roles of N6-Methyladenosine Modification in Neurodevelopment and Neurodegeneration. Cells. (2021) 10: 1-10

Sleigh J.N., Villarroel-Campos D., Surana S., Wickenden T., Tong Y., Simkin R.L., Vargas J.N.S., Rhymes E.R., Tosolini A.P., West S.J., Zhang Q., Yang X.-L., Schiavo G.: Boosting peripheral BDNF

rescues impaired in vivo axonal transport in CMT2D mice. JCI Insight. (2023) 8: 1-19

Snaidero N., Simons M.: The logistics of myelin biogenesis in the central nervous system. Glia. (2017) 65: 1021–1031

Srayko M., Kaya A., Stamford J., Hyman A.A.: Identification and characterization of factors required for microtubule growth and nucleation in the early C. elegans embryo. Developmental Cell. (2005) 9: 223–236

Ström A., Gal J., Shi P., Kasarskis E.J., Hayward L.J., Zhu H., Ström A., Gal J., Shi P., Kasarskis E.J., Hayward L.J., Zhu H.: Retrograde axonal transport and motor neuron disease. Journal of Neurochemistry. (2008) 106: 495–505

Su L.-K., Qi Y.: Characterization of human MAPRE genes and their proteins. Genomics. (2001) 71: 142–149

Sun S., Shen Y., Zhang X., Ding N., Xu Z., Zhang Q., Li L., Sun S., Shen Y., Zhang X., Ding N., Xu Z., Zhang Q., Li L., Sun S., Shen Y., Zhang X., Ding N., Xu Z., Zhang Q., Li L.: The MuSK agonist antibody protects the neuromuscular junction and extends the lifespan in C9orf72-ALS mice. Molecular Therapy. (2024) 32: 2176–2189

van de Willige D., Hoogenraad C.C., Akhmanova A.: Microtubule plus-end tracking proteins in neuronal development. Cell Mol Life Sci. (2016) 73: 2053–2077

Walker R.A., O'Brien E.T., Pryer N.K., Soboeiro M.F., Voter W.A., Erickson H.P., Salmon E.D.: Dynamic instability of individual microtubules analyzed by video light microscopy: rate constants and transition frequencies. J Cell Biol. (1988) 107: 1437–1448

Wang X., Tanaka M., Krstin S., Peixoto H.S., Moura C.C. de M., Wink M.:

Cytoskeletal interference - A new mode of action for the anticancer drugs camptothecin and topotecan. European Journal of Pharmacology. (2016) 789: 265–274

Xia L., Yin G.-L., Long Y., Sun F., Wang B.-B., Zhu Y., Chen S.-R.: The core outer junction protein CFAP77 connects A- and B-tubules within doublet microtubules of cilia and flagella. PLoS Biol. (2025) 23: 1-21

Xiao Y., Czopka T.: Myelination-independent functions of oligodendrocyte precursor cells in health and disease. Nat Neurosci. (2023) 26: 1663–1669

Yildiz A.: Mechanism and regulation of kinesin motors. Nat Rev Mol Cell Biol. (2025) 26: 86–103

Yildiz A., Zhao Y.: Dyneins. Current Biology. (2023) 33: 1274–1279

Yogev S., Cooper R., Fetter R., Horowitz M., Shen K.: Microtubule Organization

Determines Axonal Transport Dynamics. Neuron. (2016) 92: 449–460

Zanic M., Widlund P.O., Hyman A.A., Howard J.: Synergy between XMAP215 and EB1 increases microtubule growth rates to physiological levels. Nat Cell Biol. (2013) 15: 688–693

Zajt K. 2023. Modeling Neurological Diseases in Zebrafish (Danio rerio). Master's Thesis, RWTH Aachen

Zhao X., Chen X.-Q., Han E., Hu Y., Paik P., Ding Z., Overman J., Lau A.L., Shahmoradian S.H., Chiu W., Thompson L.M., Wu C., Mobley W.C.: TRiC subunits enhance BDNF axonal transport and rescue striatal atrophy in Huntington's disease. Proc Natl Acad Sci U S A. (2016). 113: 5655-5664

List of own publications

Kraft F, Rodriguez-Aliaga P, Yuan W, Franken L, Zajt K, Hasan D, Lee TT, Flex E, Hentschel A, Innes AM, Zheng B, Julia Suh DS, Knopp C, Lausberg E, Krause J, **Zhang X**, Trapane P, Carroll R, McClatchey M, Fry AE, Wang L, Giesselmann S, Hoang H, Baldridge D, Silverman GA, Radio FC, Bertini E, Ciolfi A, Blood KA, de Sainte Agathe JM, Charles P, Bergant G, Čuturilo G, Peterlin B, Diderich K, Streff H, Robak L, Oegema R, van Binsbergen E, Herriges J, Saunders CJ, Maier A, Wolking S, Weber Y, Lochmüller H, Meyer S, Aleman A, Polavarapu K, Nicolas G, Goldenberg A, Guyant L, Pope K, Hehmeyer KN, Monaghan KG, Quade A, Smol T, Caumes R, Duerinckx S, Depondt C, Van Paesschen W, Rieubland C, Poloni C, Guipponi M, Arcioni S, Meuwissen M, Jansen AC, Rosenblum J, Haack TB, Bertrand M, Gerstner L, Magg J, Riess O, Schulz JB, Wagner N, Wiesmann M, Weis J, Eggermann T, Begemann M, Roos A, Häusler M, Schedl T, Tartaglia M, Bremer J,

Pak SC, Frydman J, Elbracht M, Kurth I: Brain malformations and seizures by impaired chaperonin function of TRiC. Science. (2024) 386: 516-525.

Zhang X. *, Zajt K.K.*, Palaz T., Wang L., Groß M., Kraft F., Weis J., Bremer J.: The chaperonin TRiC component Cct3 is required for axonal transport, myelination and neuromuscular junction refinement, provisionally accepted in January 2026 at the Journal “Cell Death and Disease”

(* these authors contributed equally to this work)

Acknowledgement

The completion of this dissertation would not have been impossible without the support and assistance of many people, to whom I would like to express my sincere gratitude.

First and foremost, I would like to express my deepest gratitude to my supervisor, Professor Bremer, for her rigorous academic attitude, profound expertise, and patient guidance. She played a central role in the conception and design of this study. Her invaluable advice on research direction, methodology, and dissertation writing has greatly contributed to both the progress of this work and my academic development.

I would also like to thank my senior colleagues, Aylin Ikis, Martin Groß, Kamil Kajetan Zajt and Tayfun Palaz, for their support and assistance throughout my research. The generation of the mutant and transgenic fish lines, which formed the experimental basis of this work, was carried out by Kamil Zajt and Martin Groß. The monitoring, feeding, and administration of the

fish essential for this study were performed collaboratively by Juliane Bremer, Martin Groß, Tayfun Palaz, and Kamil Zajt, ensuring the proper maintenance of experimental conditions. Their valuable experience and constructive suggestions have been instrumental to the progress of this work. Furthermore, Juliane Bremer provided valuable support in the preparation of the German summary, while the artificial intelligence tool ChatGPT assisted with translation and language refinement.

I am also grateful to my fellow lab members, Yu Fan and Yinshuai Shang, for their helpful discussions and support. The collaborative and supportive academic environment in the lab greatly facilitated the completion of this research.

Finally, I would like to express my profound gratitude to my family for their constant understanding, support, and encouragement, which have been a solid foundation for my doctoral studies. I would also like to acknowledge myself for having the courage to

take a different way and for persevering through the challenges along the way. I hope I will always retain the courage to choose the unknown.

Erklärung zur Datenaufbewahrung

Affidavit according to § 5 (1) for Data Retention

I hereby declare that the original data forming the basis of this doctoral thesis are stored at the ***Institute of Neuropathology, University Hospital RWTH Aachen***.

Erklärung über den Eigenanteil

Eidesstattliche Erklärung gemäß § 5 Abs. (1) und § 11 Abs. (3) 12. der Promotionsordnung

Hiermit erkläre ich, **Xiaomeng Zhang** an Eides statt, dass ich folgende in der von mir selbstständig erstellten Dissertation „**Role of *cct3* in Schwann cells survival, neuromuscular junction formation as well as axonal microtubule biology and axonal transport**“ dargestellten Ergebnisse erhoben habe:
Bei der Durchführung der Arbeit hatte ich folgende Hilfestellungen, die in der Danksagung angegeben sind.

	Xiaomeng Zhang	Juliane Bremer	Künstliche Intelligenz	Tayfun Palaz	Kamil Zajt	Martin Groß	Summe (%)
Konzipierung der Studie	40	60					100
Erzeugung neuer mutanter/					67	33	100

transgener Fischlinien als Basis für die Studien							
Überwachung Fütterung und Administration der Fische, die für diese Arbeit wichtig waren	20	20		20	20	20	100
Durchführung der gezeigten Experimente	100						100
Datenerhebung	100						100
Datenauswertung inkl. Statistik	50	50					100
Zusammenfassung auf Deutsch (Übersetzung)		20	80				100

Curriculum Vitae

Xiaomeng Zhang

Basic information

Gender	female
Date of birth	15.05.1997
Place of birth	Weifang, Shandong Province, China

Education

02/2024 present	-	**Study of Neuropathology**, RWTH Aachen University, Germany
09/2020 07/2023	-	**Neurology**, Capital Medical University, Beijing, China
09/2015 07/2020	-	**Clinical Medicine** , WeiFang Medical University, Shandong, China

Research

02/2024 present	-	**Doctoral Thesis,** Institute for Neuropathology(Prof. Bremer), Medical Faculty, UKA, Title: *Role of cct3 in Schwann cells survival, neuromuscular junction formation as well as axonal microtubule biology and axonal transport*